New Phytologist

Robust anti-oxidant defences in the rice blast fungus *Magnaporthe oryzae* confer tolerance to the host oxidative burst

Marketa Samalova[1], Andreas J. Meyer[2], Sarah J. Gurr[1,3] and Mark D. Fricker[1]

[1]Department of Plant Sciences, University of Oxford, South Parks Road, Oxford, OX1 3RB, UK; [2]INRES, Universität Bonn, Friedrich-Ebert-Allee 144, D-53113 Bonn, Germany; [3]Biosciences, University of Exeter, Devon EX4 4QD, UK

Author for correspondence:
Mark D. Fricker
Tel: +44 (0)1865 275 015
Email: mark.fricker@plants.ox.ac.uk

Received: *7 June 2013*
Accepted: *20 August 2013*

New Phytologist (2014) **201:** 556–573
doi: 10.1111/nph.12530

Key words: confocal redox imaging, glutathione, Grx1-roGFP2, *Magnaporthe oryzae*, mitochondrial activity, monochlorobimane, reactive oxygen species (ROS), rice blast pathogen response.

Summary

- Plants respond to pathogen attack via a rapid burst of reactive oxygen species (ROS). However, ROS are also produced by fungal metabolism and are required for the development of infection structures in *Magnaporthe oryzae*.
- To obtain a better understanding of redox regulation in *M. oryzae*, we measured the amount and redox potential of glutathione (E_{GSH}), as the major cytoplasmic anti-oxidant, the rates of ROS production, and mitochondrial activity using multi-channel four-dimensional (*x,y,z,t*) confocal imaging of Grx1-roGFP2 and fluorescent reporters during spore germination, appressorium formation and infection.
- High levels of mitochondrial activity and ROS were localized to the growing germ tube and appressorium, but E_{GSH} was highly reduced and tightly regulated during development. Furthermore, germlings were extremely resistant to external H_2O_2 exposure *ex planta*. E_{GSH} remained highly reduced during successful infection of the susceptible rice cultivar CO39. By contrast, there was a dramatic reduction in the infection of resistant (IR68) rice, but the sparse hyphae that did form also maintained a similar reduced E_{GSH}.
- We conclude that *M. oryzae* has a robust anti-oxidant defence system and maintains tight control of E_{GSH} despite substantial oxidative challenge. Furthermore, the magnitude of the host oxidative burst alone does not stress the pathogen sufficiently to prevent infection in this pathosystem.

Introduction

Rice blast disease caused by *Magnaporthe oryzae* is a major global emerging infectious disease (EID) causing rice losses sufficient to feed 3–10.6% of the world's population 2000 calories a day for 1 yr (Fisher *et al.*, 2012). Infection starts with the germination of a three-celled spore on the host surface, producing a short germ tube that develops a domed infection structure, termed the appressorium (Wilson & Talbot, 2009). Development requires progression through a single cell cycle in the apical cell, followed by autophagy (Veneault-Fourrey *et al.*, 2006) and mobilization of storage reserves to fuel appressorium development (Thines *et al.*, 2000; Wang *et al.*, 2007; Patkar *et al.*, 2012a). The appressorium becomes melanized and builds up sufficient turgor pressure to drive an infection peg into the host epidermal cell (Howard *et al.*, 1991; Money & Howard, 1996; Wilson & Talbot, 2009). In a susceptible host, the infection hyphae ramify through the infected cell and then colonize adjacent cells through plasmodesmata (Kankanala *et al.*, 2007). In resistant varieties, infection is halted at the penetration stage or during early colonization, and is associated with a hypersensitive response (HR) (Torres, 2010; Heller & Tudzynski, 2011).

Plants respond to infection by the rapid production of reactive oxygen species (ROS) using membrane-bound NADPH oxidases (Marino *et al.*, 2012), or secreted peroxidases and amine oxidases (Bolwell *et al.*, 2002), as part of the general pathogen-associated molecular pattern (PAMP)-triggered immunity (PTI) or more specific effector-triggered immunity (ETI) responses (Yoshioka *et al.*, 2009; Torres, 2010; Heller & Tudzynski, 2011; Thomma *et al.*, 2011; Tudzynski *et al.*, 2012). ROS produce cross-linked plant wall polymers to form a barrier to penetration, attack the pathogen directly or act as diffusible signals in the plant to up-regulate pathogenesis-related proteins (Lamb & Dixon, 1997; Shetty *et al.*, 2008; Heller & Tudzynski, 2011). In a resistant host challenged by an avirulent pathogen, the initial ROS burst is followed by a longer lasting second phase, culminating in an HR (Mur *et al.*, 2008) and programmed cell death (Levine *et al.*, 1994). In biotrophic and hemibiotrophic fungi, such as *M. oryzae*, which require living hosts, the first phase of ROS production still occurs, but the second phase is suppressed in susceptible hosts, probably through the secretion of effectors through the biotrophic interfacial complex (Valent & Khang, 2010), which re-programme the metabolic pathways involved in host ROS production (Parker *et al.*, 2009).

Fungi require effective anti-oxidant defence systems to operate in such an environment in which oxidative stress is endemic. An abundant array of anti-oxidant genes exists in the *M. grisea* genome (Dean *et al.*, 2005; Egan & Talbot, 2008; Morel *et al.*, 2008), although less is known about the low-molecular-weight anti-oxidants in fungi more generally (Georgiou & Petropoulou, 2001; Patsoukis & Georgiou, 2004). Nevertheless, the need to detoxify host ROS can be inferred from fungal mutants that lack critical anti-oxidant enzymes, or from treatments that manipulate ROS levels during infection. Thus, *Magnaporthe* mutants in glutathione peroxidase, Hyr1, are less tolerant to ROS and produce smaller lesions on susceptible plants (Huang *et al.*, 2011). Likewise, several redox-sensitive transcription factors, such as MoAP1 (Guo *et al.*, 2011) and MoSwi6 (Qi *et al.*, 2012), and the defence suppressor Des1 (Chi *et al.*, 2009) increase resistance to external H_2O_2, with mutants showing reduced pathogenicity and pleiotropic changes in gene expression, including decreases in extracellular peroxidases. Conversely, the reduction of external ROS levels during infection through the addition of exogenous catalase (Tanabe *et al.*, 2009) or the NADPH oxidase inhibitor diphenylene iodonium (DPI) (Chi *et al.*, 2009) promotes increased infection of compatible and incompatible strains, or particular H_2O_2-sensitive mutants.

Nevertheless, the significance of other putative anti-oxidant defences is less clear. Thus, the deletion of the major secreted *M. oryzae* catalase-peroxidase, CPXB, increases sensitivity to exogenous H_2O_2, but does not affect overall pathogenicity (Tanabe *et al.*, 2011). Likewise, mutants lacking the large subunit catalase, catB, are less pathogenic, but through changes in normal fungal wall strengthening rather than by detoxification of host-derived H_2O_2 (Skamnioti *et al.*, 2007). Furthermore, expression data from transcriptome profiling show that the genes most highly up-regulated in *M. oryzae* during infection are related to nutrient limitation rather than oxidative stress (Mathioni *et al.*, 2011). This echoes results for the necrotrophic fungus *Botrytis cinerea*, in which the redox-sensitive AP1 transcription factor homologue, Bap1, is critical for ROS resistance *in vitro*, but deletion mutants do not show reduced virulence, and the suite of downstream target genes regulated by Bap1 is not highly expressed *in planta* (Temme & Tudzynski, 2009). The authors concluded that *B. cinerea* does not suffer H_2O_2 stress *in planta*, in contrast with conventional expectations of the role of the oxidative burst in restricting infection (Temme & Tudzynski, 2009), but actually exploits the host HR as part of its necrotrophic habit (Govrin & Levine, 2000).

The interplay between ROS and anti-oxidant defences is further complicated, as ROS are produced by normal cell metabolism and act as signalling intermediates associated with key transitions in microbial development, including differentiation, sexual reproduction, conidiation, spore germination, secondary metabolism and apoptosis (Hansberg & Aguirre, 1990; Aguirre *et al.*, 2005; D'Autreaux & Toledano, 2007; Gessler *et al.*, 2007; Takemoto *et al.*, 2007; Egan & Talbot, 2008; Scott & Eaton, 2008; Shetty *et al.*, 2008; Aguirre & Lambeth, 2010; Heller & Tudzynski, 2011; Tudzynski *et al.*, 2012). Indeed, Hansberg and Aguirre originally proposed that microbial cell differentiation might be triggered by transient oxidation that initiates a shift between developmental states (Hansberg & Aguirre, 1990; Aguirre *et al.*, 2005). ROS production is well documented during pre-penetration in *M. oryzae*, whereas scavenging external ROS reduces infection rates, all consistent with a role for ROS in the developmental programme (Egan *et al.*, 2007; Ryder *et al.*, 2013).

The major cytoplasmic anti-oxidant that mitigates oxidative stress in eukaryotes is glutathione (Belozerskaya & Gessler, 2007; Gessler *et al.*, 2007; Meyer, 2008). However, little is known about the glutathione concentrations and dynamics in filamentous fungi. Tools are now available to quantify both the amount of glutathione *in vivo* (Fricker *et al.*, 2000; Meyer & Fricker, 2000, 2008; Fricker & Meyer, 2001; Meyer *et al.*, 2001) and the electrochemical potential of the reduced glutathione:oxidized glutathione (GSH:GSSG) redox couple (E_{GSH}) using transgenic redox green fluorescent protein (GFP)-based reporters (Dooley *et al.*, 2004; Schwarzlander *et al.*, 2008; Meyer & Dick, 2010). In particular, Grx1-roGFP2 includes a glutaredoxin (Grx) subunit to improve the response kinetics (Gutscher *et al.*, 2008) and is known to function correctly in fungi (Heller *et al.*, 2012). Notably, the difference in the mid-point potential between the Grx1-roGFP redox couple and the GSH:GSSG redox couple makes Grx1-roGFP exquisitely sensitive to small changes in the degree of glutathione oxidation from the highly reduced level typically found *in vivo* (Meyer & Dick, 2010). Thus, in this article, we use multi-parameter live-cell confocal imaging and a range of fluorescent reporters to determine, first, whether there is physiological evidence for the redox control of early development in *M. oryzae* mediated by changes in E_{GSH}; second, what is the relative level of endogenous ROS production during development; third, what is the capacity of the glutathione anti-oxidant system to deal with an imposed oxidative burst, as might be encountered during host infection; and fourth, what impact is exerted by the actual host oxidative burst on E_{GSH} *in vivo* during susceptible and resistant interactions.

Materials and Methods

Fungal strains and growth conditions

Wild-type *Magnaporthe oryzae* strain Guy11 and transgenic Grx1-roGFP2 strain were cultured at 24°C under a 14 h : 10 h light : dark cycle according to Talbot *et al.* (1993). Spores were scraped from 10-d-old cultures, filtered through two layers of miracloth (Calbiochem, San Diego, CA, USA), washed with sterile demineralized water (dH_2O), pelleted by centrifugation (4000 ***g***, 5 min) and resuspended in dH_2O at a spore concentration of *c.* 5×10^5 ml^{-1}.

Cloning and generation of pRP27::Grx1:roGFP2 strains

Standard molecular techniques and cloning (Ausubel *et al.*, 1999) were used to prepare the pRP27::Grx1:roGFP2 construct. A set of transformation vectors was created based on pUCAP (van Engelen *et al.*, 1995), which carries pUC19 MCS and unique *Asc*I and *Pac*I sites.

The bialophos resistance marker (GenBank AF013602) was removed as a *Sal*I fragment from pGEMTEasy-BAR vector (Samalova *et al.*, 2013), blunt-ended and cloned into the pUCAP *Sac*I site, and digested with *Ecl*136II to re-create the *Sal*I sites and generate pUCAP-BAR. The polyadenylation signal pATrpC was amplified from pMJK142.2 (kindly provided by Professor N. Talbot, Exeter, UK) using P1 and P2 primers (Table 1), digested with *BamH*I and *Kpn*I, and cloned into the same restriction sites of the pUCAP-BAR vector, creating pUCAP-pATrpC/BAR, and confirmed by sequencing. The *M. oryzae* promoter RP27 (Czymmek *et al.*, 2002) was amplified from Guy11 genomic DNA using P3 and P4 primers (Table 1). Grx1-roGFP2 was amplified from pBinCM-GRX1-roGFP2 (Gutscher *et al.*, 2008) using P5 and P6 primers (Table 1). The two fragments were fused by overlapping PCR using primers P3 and P6. The PCR product was digested with *Asc*I and *Bam*HI, and cloned into the same restriction sites of pUCAP-pATrpC/BAR. The final pUCAP-pRP27::Grx1:roGFP2 vectors were confirmed by sequencing, and digested with *Pac*I, before transformation into *M. oryzae*.

DNA-mediated protoplast transformation (Talbot *et al.*, 1993) was used to generate putative transformants that were selected on defined complex medium supplemented with 60 μg ml^{-1} bialophos (Goldbio, St Louis, MO, USA). They were subjected to PCR using P6 and P7 primers (Table 1) to confirm the presence of Grx1-roGFP2. The most fluorescent line was chosen for this study.

Leaf sheath assays

Rice cultivar CO39 (susceptible) and IR68 (resistant; Gilbert *et al.*, 2006; Hubbart *et al.*, 2007) were grown at 24°C, 80% humidity in a 14 h light cycle. Leaf sheaths of 2–3-wk-old plants were inoculated with 20–40 μl of conidial suspension (5×10^5 spores ml^{-1}) and placed onto water agar (2% w/v) in the growth chamber. Leaf sheaths were mounted using double-sided tape, sliced open with a razor blade and imaged by confocal microscopy.

Confocal imaging

Time series were collected at 30–120-s intervals for 15–45 min, as *z*-stacks of 5–10 sections taken at 0.67–3-μm intervals apart, using a Zeiss 40× 1.2 NA PlanApo water-immersion lens. Pixel sizes were 0.22–0.44 μm in *x* and *y*. Pinhole settings were adjusted individually for each channel to give an estimated optical section thickness of 2–3 μm (*c.* 2–3 Airy units) for each of the wavelength combinations. This provided some degree of optical sectioning, but with sufficient signal-to-noise to allow long-term physiological measurements with low laser intensities. Laser power was measured from the defocused beam using a Newport 1815-C power meter (Newport Corp., Irvine, CA, USA). Values ranged from 1.3 to 7.3 μW. Non-confocal bright-field images were collected simultaneously with a transmission detector.

Coverslips were placed in a perfusion chamber mounted on a Zeiss LSM510META confocal microscope and Grx1-roGFP2 (emission, 505–530 nm) was imaged with 405- and 488-nm excitation in multi-track mode with line switching. Autofluorescence was measured in parallel (excitation, 405 nm; emission, 435–485 nm).

Table 1 List of primers (5′–3′)

P1:	AAAAGGATCCGCGGCCGCTACGTAATTTAAATACTTAACGTTACTGAAATCATCAAACAG
P2:	AAAAGGTACCGGCCCTAGGGGCCAGATGTGGAGTGGGCGCTTACACAG
P3:	AAAAGGCGCGCCATAAATGTAGGTATTACCTGTACATTTTATTTATTC
P4:	CATTTTGAAGATTGGGTTCCTACGAAAGC
P5:	CGCCTAACAGATCTTGGCTTTCGTAGGAACCCAATCTTCAAAATGGCTCAAGAGTTTGTGAACTGC
P6:	AAAAGGATCCTTACTTGTACAGCTCGTCCATGCCG
P7:	AAAAACCATGGCTCAAGAGTTTGTGAACTGC

Dual-excitation confocal ratiometric analysis

Image time series were imported into a custom MatLab (The MathWorks, Natick, MA, USA) program (available on request from M.D.F.). *z*-stacks were averaged in *x*, *y* and *z* using a $3 \times 3 \times 3$ or $5 \times 5 \times 3$ kernel. The *z*-position of the brightest pixel in a maximum *z*-projection of the main channel of interest was used to extract the corresponding *z*-pixel for each of the other wavelengths to give the average intensity from all channels in a volume around the same, bright pixel in *x*, *y* and *z*. The resultant image is termed an optimum plane projection. The average background intensity was measured adjacent to the spores on coverslips, or in the vacuole for *in planta* experiments, and subtracted. The autofluorescence bleed-through contribution into the Grx1-roGFP2$_{405}$ channel was measured from Guy11 spores, and the corresponding scaling factor was used to subtract autofluorescence from the Grx1-roGFP2$_{405}$ image. Ratio images were calculated on a pixel-by-pixel basis as I_{405}/I_{488}. Pixels with intensity values < 2 standard deviation units above background, within 10% of saturation, or where the local coefficient of variance (CV) in a 3×3 neighbourhood was above 20%, were masked.

For pseudo-colour display, the masked ratio was coded by hue on a spectral colour scale ranging from blue (most reduced) to red (most oxidized), with the limits set by the *in situ* calibration. Individual germlings were segmented using Otsu's method (Otsu, 1979) and the extracted images were rotated to give a montage of selected time points for display.

Quantitative measurements were calculated as the ratio of the mean intensity from each channel from the regions of interest. *In situ* calibration was performed using 10 mM dithiothreitol (DTT) for 5 min, followed by 100 mM H_2O_2 for 5 min, to drive Grx1-roGFP2 to a highly reduced and highly oxidized form, respectively. The degree of oxidation ($OxD_{Grx1\text{-}roGFP2}$) and pH-corrected GRx1-roGFP redox potential ($E_{Grx1\text{-}roGFP2}$) were calculated according to Schwarzlander *et al.* (2008), assuming a mid-point potential ($E^{o}_{Grx1\text{-}roGFP2}$) of −280 mV (Dooley *et al.*, 2004; Hanson

et al., 2004; Gutscher *et al.*, 2008; Morgan *et al.*, 2011, 2013) and a cytoplasmic pH of pH 7.6 (Parton *et al.*, 1997; Hesse *et al.*, 2002).

For population studies, a Gaussian mixture model (GMM) with two to four components was fitted to the pixel intensities at each wavelength, with the contribution of each pixel weighted by the average intensity. Contour maps from the GMM were overlaid on two-dimensional histograms generated from the weighted pixel intensities. The intensity value of the Gaussian peak at each wavelength was used to calculate the ratio, and hence degree of Grx1-roGFP2 oxidation, $E_{\text{Grx1-roGFP2}}$ and E_{GSH}, respectively, for each component.

Estimation of cytosolic glutathione concentrations in spores of *M. oryzae*

The available glutathione pool was labelled *in situ* following conjugation to 100 μM monochlorobimane (MCB) to give a fluorescent glutathione–bimane (GSB) conjugate (excitation, 405 nm; emission, 435–485 nm) according to Fricker *et al.* (2000), Fricker & Meyer (2001), Meyer *et al.* (2001) and Meyer & Fricker (2002). Calibration solutions were made by reacting 10 mM monobromobimane with an excess of GSH. As GSB was transported into the vacuole, estimation of the initial cytosolic GSH concentration required correction for the cytoplasmic : vacuolar volume ratio. GSB signals from overlapping vacuoles were separated using a three-dimensional watershed and the regional maximum intensity for each vacuole was determined. Each vacuolar volume was estimated as the number of pixels above the 50% threshold between this local maximum and the background (White *et al.*, 1996; Errington *et al.*, 1997).

The cytoplasmic volume was the difference in volume between the vacuole volume and the total volume of the spore compartment, estimated after labelling the cell wall with 15 μM propidium iodide (PI; excitation, 543 nm; emission, 585–6150 nm). Three-dimensional *z*-stacks were rotated in *x, y* and tilted in *z* to align the long axis of the spore with the *x*-axis. The median wall outline was segmented from the maximum z-projection, filled and the volume was measured assuming radial symmetry from the cylinder of rotation about the *x*-axis.

Measurement of ROS levels and mitochondrial activity

Spores were labelled with 0.2–2.5 μM 2′,7′-dichlorodihydrofluorescein diacetate (H_2DCFDA) (excitation, 488 nm; emission, 500–530 nm) or CellROX Deep Red (CRDR, 2.5 μM) simultaneously with tetramethyl rhodamine methyl ester (TMRM, 100 nM) for mitochondria, and Grx1-roGFP2 for GSH redox potential, using quadruple excitation with paired line switching at 405 and 633 nm, and 488 and 543 nm. Emission wavelengths were 435–485, 500–530 and 657–721 nm for wall autofluorescence, oxidized Grx1-roGFP2 and CRDR, respectively, and 500–530 nm and 561–603 nm for reduced Grx1-roGFP2 and TMRM, respectively. A non-confocal, bright-field transmission image was collected in parallel.

Results and Discussion

Grx1-roGFP2 reports E_{GSH} in *M. oryzae*

To measure the electrochemical potential of the GSH:GSSG redox couple (E_{GSH}) *in vivo*, Grx1-roGFP2 (Gutscher *et al.*, 2008; Heller *et al.*, 2012) was expressed from the ribosomal protein RP27 promoter in *M. oryzae* and visualized using confocal ratio imaging (Meyer & Fricker, 2008; Schwarzlander *et al.*, 2008; Morgan *et al.*, 2011). Spores expressing Grx1-roGFP2 showed normal rates of germ tube extension, swelling and appressorium development (e.g. Fig. 1e), and were fully pathogenic on barley and rice (data not shown). Fluorescence was observed in the cytoplasm and, to a lesser extent, vacuoles (Fig. 1a–d, Supporting Information Video S1). Excitation at 405 nm increased with probe oxidation, but also caused autofluorescence bleed-through into the Grx1-roGFP2$_{405}$ channel, typically around the site of germ tube emergence and the appressorium wall. To correct the Grx1-roGFP2$_{405}$ images, autofluorescence images were collected at 435–485 nm (Fig. 1f), scaled by an empirically determined bleed-through correction factor and subtracted. Localization of Grx1-roGFP2 in vacuoles was not expected, but parallels other cytoplasmically expressed fluorescent proteins in *M. oryzae* germlings, such as mCherry (data not shown, see also Czymmek *et al.*, 2002), and may reflect high levels of autophagy. Nevertheless, the Grx1-roGFP2 signal in both cytoplasmic and vacuolar compartments responded to *in situ* calibration (Fig. 1g,h). Changes in the Grx1-roGFP2 spectrum were visualized as pseudo-colour-coded ratio images, scaled to the minimum and maximum of these calibration values (Fig. 1i).

Grx1-roGFP2 responses were rapid, with oxidation by H_2O_2 within 1–2 min, and reversible, with spontaneous recovery to a reduced state after washout (Fig. 1j–l), and reduction with subsequent exposure to DTT (Fig. 1j–l). Although H_2O_2 caused bleaching of the probe (Fig. 1j,k), the ratio corrected for the changes in intensity (Fig. 1l), giving a dynamic range around four, similar to previous reports with the wavelength combinations used here (Gutscher *et al.*, 2008). It is notable that *M. oryzae* was very resistant to imposed oxidative loads, with 100 mM H_2O_2 needed to drive Grx1-roGFP2 to an oxidized state *in vivo*. Using this calibration, the degree of oxidation of cytoplasmic Grx1-roGFP2 ($\text{OxD}_{\text{Grx1-roGFP2}}$) was 10–12% in all three germling cells (Fig. 1m). Interestingly, vacuolar Grx1-roGFP2 still responded to calibration, with the same dynamic range, giving a value equivalent to 50–60% oxidation (Fig. 1d,k,l). $\text{OxD}_{\text{Grx1-roGFP2}}$ was converted to the redox potential ($E_{\text{Grx1-roGFP}}$) (Gutscher *et al.*, 2008; Schwarzlander *et al.*, 2008; Meyer & Dick, 2010) using a consensus mid-point potential ($E^{\prime}{}_{\text{Grx1-roGFP2}}$) of −280 mV (Dooley *et al.*, 2004) and a cytoplasmic pH of pH 7.6, as measured in filamentous fungi (Parton *et al.*, 1997; Hesse *et al.*, 2002). With these assumptions, 10% oxidation of Grx1-roGFP2 equates to $E_{\text{Grx1-roGFP2}}$ of −316 mV. Assuming that $E_{\text{Grx1-roGFP2}}$ equilibrates with E_{GSH} (Morgan *et al.*, 2011), this requires tight regulation of GSSG at submicromolar concentrations (Meyer & Dick, 2010; Morgan *et al.*, 2013). Thus, we infer that Grx1-roGFP2 provides a rapid and highly sensitive readout *of* E_{GSH} in

M. oryzae, similar to previous reports for the necrotrophic fungus *B. cinerea* (Heller *et al.*, 2012). Nevertheless, high-resolution imaging is also required to separate signals from cytoplasm and vacuole.

The glutathione pool shows only slight shifts in the degree of oxidation during development

To determine whether there were shifts in glutathione oxidation associated with developmental transitions (Hansberg & Aguirre, 1990), we quantified $OxD_{Grx1\text{-}roGFP2}$ at different developmental stages, classified as: spores (0–0.5 h post-inoculation, hpi), germination (0.5–1 hpi), germ tube growth (1–2 hpi), germ tube swelling (2–3 hpi), appressorium formation (3–5 hpi) and appressorial melanization (5–8 hpi).

A highly reduced cytoplasmic Grx1-roGFP2 signal (< 5% oxidized) was measured during germination in all three spore cells (Fig. 2i), becoming slightly more oxidized (8–12%) as the germ tube developed at 1–2 hpi (Fig. 2a,b,i, see also Fig. 1). Ratios from the mid and basal cells were progressively dominated by the oxidized Grx1-roGFP2 vacuolar signal once appressoria started to form at 5 hpi (Fig. 2c,d,i), making it difficult to extract a clean cytoplasmic value. Absolute fluorescence intensities were also reduced from the basal and mid cells *c.* 8 hpi (Fig. 2e,f), and disappeared following isolation and autophagic cell death at 24 hpi (Fig. 2g,h). At this stage, the apical cell was more vacuolate, but the cytoplasmic probe was still responsive to calibration. The appressorium itself showed a highly reduced cytoplasmic Grx1-roGFP2 signal throughout development, with a characteristic ring of more oxidized vacuoles around the periphery (Fig. 2f,h,i). However, Grx1-roGFP2 in the melanizing appressorium (Fig. 2f) was protected from H_2O_2 calibration, with slower responses at 8 hpi and complete insensitivity to 100 mM H_2O_2 at 24 hpi (Fig. 2 h).

We infer that *M. oryzae* maintains a highly reduced cytoplasmic E_{GSH} during early development, and there was only very limited evidence that E_{GSH} increases during appressorium formation, indicative of a glutathione-mediated redox-associated developmental switch (Hansberg & Aguirre, 1990).

There are high levels of endogenous ROS production during development

In the absence of a host, E_{GSH} reflects the rate of detoxification of endogenous metabolic ROS. Previous measurements of ROS levels in *M. oryzae* have used the relatively non-specific probe

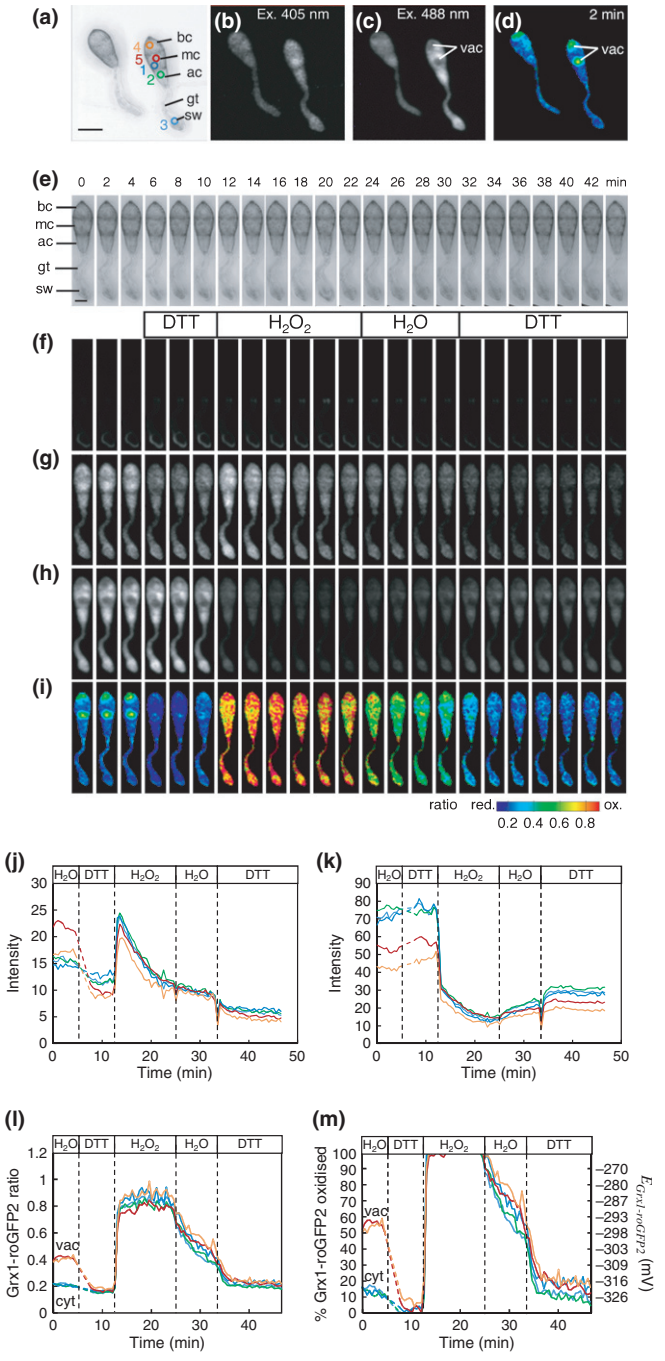

Fig. 1 Measurement of the redox potential of the glutathione pool in *Magnaporthe oryzae* germlings using recombinant Grx1-roGFP2. Germinating spores of *M. oryzae* (a, e) expressing Grx1-roGFP2 from the RP27 promoter were sequentially imaged with excitation at 405 nm (b, g) and 488 nm (c, h) as z-stacks with 2-μm spacing at 60-s time intervals, and analysed as optimum plane projections (g, h) after smoothing with a 3 × 3 averaging filter and correction for bleed-through from autofluorescence (f) in the 405-nm channel. Grx1-roGFP2 was located predominantly in the cytoplasm of the basal cell (bc), mid cell (mc) and apical cell (ac), including the germ tube (gt) and swelling germ tube tip (sw). Fluorescence was also observed in the vacuole (vac), particularly in the basal and mid cells. The degree of oxidation of Grx1-roGFP2 was visualized from the pseudo-colour-coded ratio (d, i), following calibration with 10 mM dithiothreitol (DTT) to reduce the internal pool, and 100 mM H_2O_2 to oxidize it (f–i). Although the cytoplasm showed a uniform low ratio, Grx1-roGFP2 ratios from the vacuoles indicated that the probe was more oxidized, but still capable of responding to calibration (i). To quantify the responses, the average fluorescence from regions of interest in (a) were measured for excitation at 405 nm (j) and 488 nm (k), with the corresponding ratio (l) and conversion to the degree of oxidation of the GRx1-roGFP probe ($OxD_{Grx1\text{-}roGFP2}$) (m). The corresponding redox potential ($E_{Grx1\text{-}roGFP2}$) was calculated using $E^{o\prime}_{Grx1\text{-}roGFP2} = -280$ mV and a cytoplasmic pH of pH 7.6 (m). Assuming that the Grx1-roGFP redox couple is in equilibrium with the GSH:GSSG redox couple, E_{GSH} is equal to $E_{Grx1\text{-}roGFP2}$. Bar, 10 μm. See Supporting Information Video S1 for a movie of the complete time series.

H_2DCFDA (Egan *et al.*, 2007; Kim *et al.*, 2009; Guo *et al.*, 2011; Huang *et al.*, 2011). H_2DCFDA is membrane permeant, but trapped intracellularly following the cleavage of the di-acetate groups by intracellular esterases, where oxidation gives fluorescent 2′,7′-dichlorofluorescein (DCF). Nevertheless, it is not clear to which ROS the probe responds, as intrinsic reaction rates with H_2O_2 and superoxide are low, and the probe is likely to be oxidized by more reactive species or through the action of peroxidases or haem proteins (Halliwell & Whiteman, 2004; Rhee *et al.*, 2010).

DCF fluorescence accumulated mainly in the cytoplasm in all three cells at all stages of germling development (Fig. 3b,d, see also Video S2). The greatest increase in fluorescence was observed in the mid cell (Fig. 3e,f), at about twice the rate in the other cells. Significant DCF also accumulated in the appressorium wall (Fig. 3d,f, see also Video S2). These data are similar to previous reports of DCF staining in conidia and in septal cell walls before germination, followed by labelling in germ tubes and a burst during appressorium formation, which might reflect the activity of the Nox1 NADPH oxidase (Egan *et al.*, 2007; Ryder *et al.*, 2013). However, this would also imply that there was sufficient de-esterified H_2DCF in the apoplast to react with externally produced ROS.

Washout of the labelling medium led to rapid loss of the wall-associated label, consistent with free dye in the apoplast (Fig. 3d, f). However, there was also substantial loss of cytoplasmic fluorescence in all three cell types, together with some recovery in the appressorial wall (Fig. 3d,f). We infer that DCF is either very membrane permeant in *M. oryzae*, or there is an additional plasma membrane xenobiotic detoxification system, which would also explain the inverse kinetics of cytoplasmic and wall signals during washout (Fig. 3d,f). Previously, we have reported a similar phenomenon for the NO reporter diaminorhodamine-4M (DAR-4M) in *M. oryzae* (Samalova *et al.*, 2013). Indeed, *Magnaporthe* is well endowed with potential transporters, with 50 members of the ATP-binding cassette (ABC) transporter family and 251 members of the major facilitator superfamily (MFS)

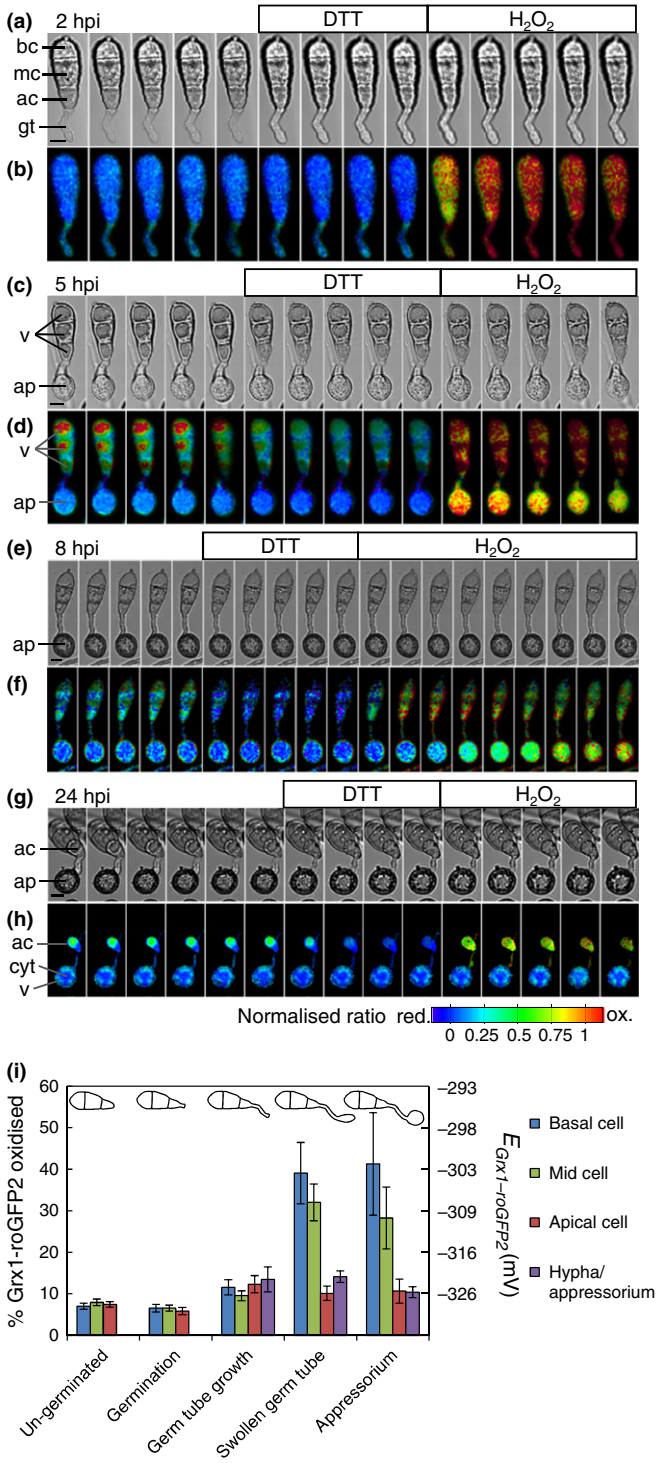

Fig. 2 Glutathione redox potential during development in different cell types of *Magnaporthe oryzae*. The degree of oxidation of Grx1-roGFP ($OxD_{Grx1\text{-}roGFP2}$) was calculated for each cell type in spores and developing germlings, following calibration with dithiothreitol (DTT) and H_2O_2. $OxD_{Grx1\text{-}roGFP2}$ was low in un-germinated and germinating spores, with average values of *c.* 6% ($n = 15$) and 4% ($n = 12$), respectively), in each cell type (i), but rose slightly to *c.* 8–12% during germ tube growth (a, b, i, $n = 10$). This corresponds to a shift of only a few millivolts (mV) in redox potential (i). Around 3–5 h post-inoculation (hpi), when germ tubes began to swell and form appressoria, the signal from the basal cell (bc) and mid cell (mc) was dominated by the vacuole, with a corresponding higher resting level of oxidation (c, d, i, $n = 13$), that prevented the measurement of a true cytoplasmic ratio. At 8 hpi, the appressorium only responded slowly to the calibration solutions, even with extended incubation (e, f, $n = 9$). Signals from the basal cell and mid cell were weak (f), and much more oxidized (i). By 24 hpi, when the appressorium was melanized (g), there was essentially no signal from the basal or mid cell, whereas the apical cell started to become vacuolated. Grx1-roGFP2 in the cytoplasm in the appressorium remained highly reduced (*c.* 8% oxidized), but was *c.* 40% oxidized in the small ring of vacuoles around the periphery (h). The signal in the apical cell still responded to calibration (h). However, Grx1-roGFP2 in the appressorium was effectively insulated from the calibration solutions at this developmental stage (h). Fluorescent images are shown as optimum plane projections of each z-stack (a–f) or every other z-stack (g, h), following smoothing with a 3 × 3 × 3 spatial average and autofluorescence correction, from a multi-channel (*x*,*y*,*z*,*t*) four-dimensional image series collected at 60-s intervals. The bright-field image was a minimum projection of the non-confocal transmission images collected in parallel. ac, apical cell; ap, appressorium; cyt, cytoplasm; gt, germ tube; v, vacuole. Results are presented as mean ± SEM. Bars, 5 μm.

New Phytologist

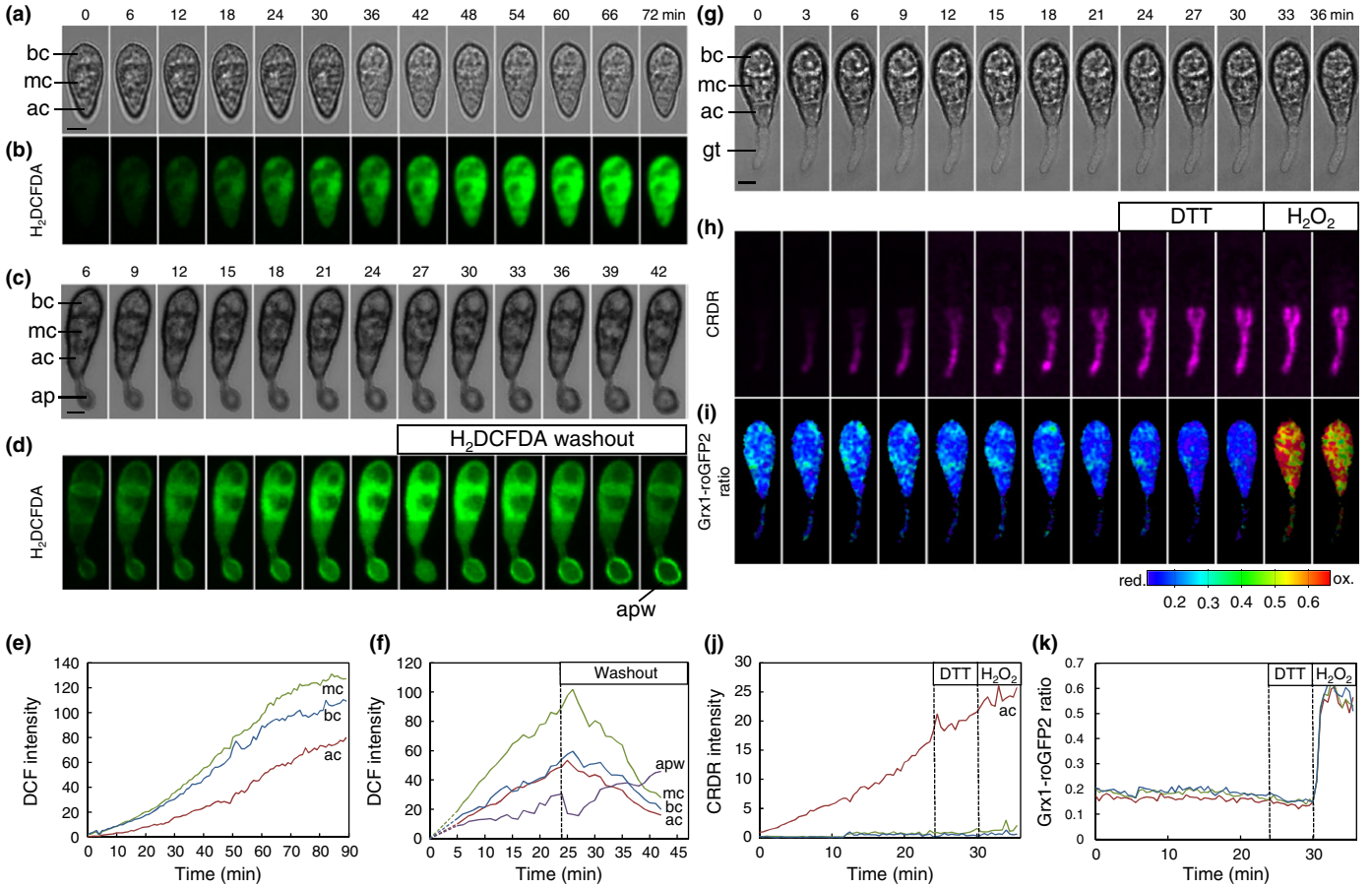

Fig. 3 Endogenous reactive oxygen species (ROS) production during development in *Magnaporthe oryzae*. Germlings of *M. oryzae* were labelled with 2′,7′-dichlorodihydrofluorescein diacetate (H_2DCFDA), as a non-specific reporter for ROS, at different stages of development. Fluorescent signals increased in all three cell types during germination (a, b, e) and appressorium formation (c, d, f), with signal also appearing in the appressorium cell wall (apw) (d, f). In the continuous presence of dye in the medium, labelling rates showed some sigmoidicity during germination (e), but were approximately linear at subsequent time points (f), with the highest rate in the mid cell (mc). However, replacement of the dye loading solution led to rapid loss of signal from the appressorium cell wall, followed by the apical cell (ac) with a delay of *c*. 1 min, and then the mid (mc) and basal (bc) cells after 2–3 min (d, f). CellROX Deep Red (CRDR) was used as an alternative ROS sensor as it can be used in conjunction with Grx1-roGFP2 (g–k). CRDR showed strong labelling of punctate tubular structures in the apical cell (g, h) that increased linearly over time (j), with only weak diffuse signal from the other cells in the germling (h, j). The ratio from Grx1-roGFP2 was close to a fully reduced state (i, k). Fluorescence images are shown as maximum (b,d) or optimum plane (h,i) *z*-projections, following smoothing with a 3 × 3 × 3 spatial average, of every third (a–d) or sixth (g–i) *z*-stack from multi-channel four-dimensional (*x*,*y*,*z*,*t*) images collected at 60- or 30-s intervals, respectively. Bright-field images are mid-sections from the non-confocal transmission images collected in parallel. Bars, 5 μm. See Video S2 for a movie of the complete time series.

(Coleman & Mylonakis, 2009). Furthermore, several of these transporters are up-regulated during appressorium formation (Oh *et al.*, 2008), under stress treatments or *in planta* (Mathioni *et al.*, 2011), and are required for pathogenicity (Urban *et al.*, 1999; Sun *et al.*, 2006; Patkar *et al.*, 2012b), possibly to protect against the buildup of peroxides and oxidative damage (Sun *et al.*, 2006).

Given our concerns over H_2DCFDA localization and specificity, we also examined the more sensitive, specific and photostable long-wavelength ROS probe CRDR. CRDR showed a time-dependent increase in fluorescence in *M. oryzae* spores, but, by contrast with H_2DCFDA, CRDR labelled discrete punctate structures, predominantly in the apical cell (Fig 3h,j). Despite this apparent asymmetric ROS production, simultaneous imaging with Grx1-roGFP2 showed a consistent low ratio in all three cell types (Fig. 3k). We speculate that CRDR might highlight mitochondrial ROS production, and probably reacts with superoxide rather than H_2O_2, given the lack of response to H_2O_2 addition (Fig. 3k).

Mitochondria show different activity in each germling cell type during development

To investigate whether the increase in CRDR fluorescence principally reflects the high level of ROS produced by mitochondrial activity (Schwarzlander & Finkemeier, 2013), we tested whether the punctate CRDR structures co-localized with active mitochondria, identified by potential-dependent accumulation of TMRM, and whether the mitochondria were differentially active in the different spore cells. In addition, we examined whether there were any changes in mitochondrial ROS production associated with developmental switches, particularly as mitochondria are involved

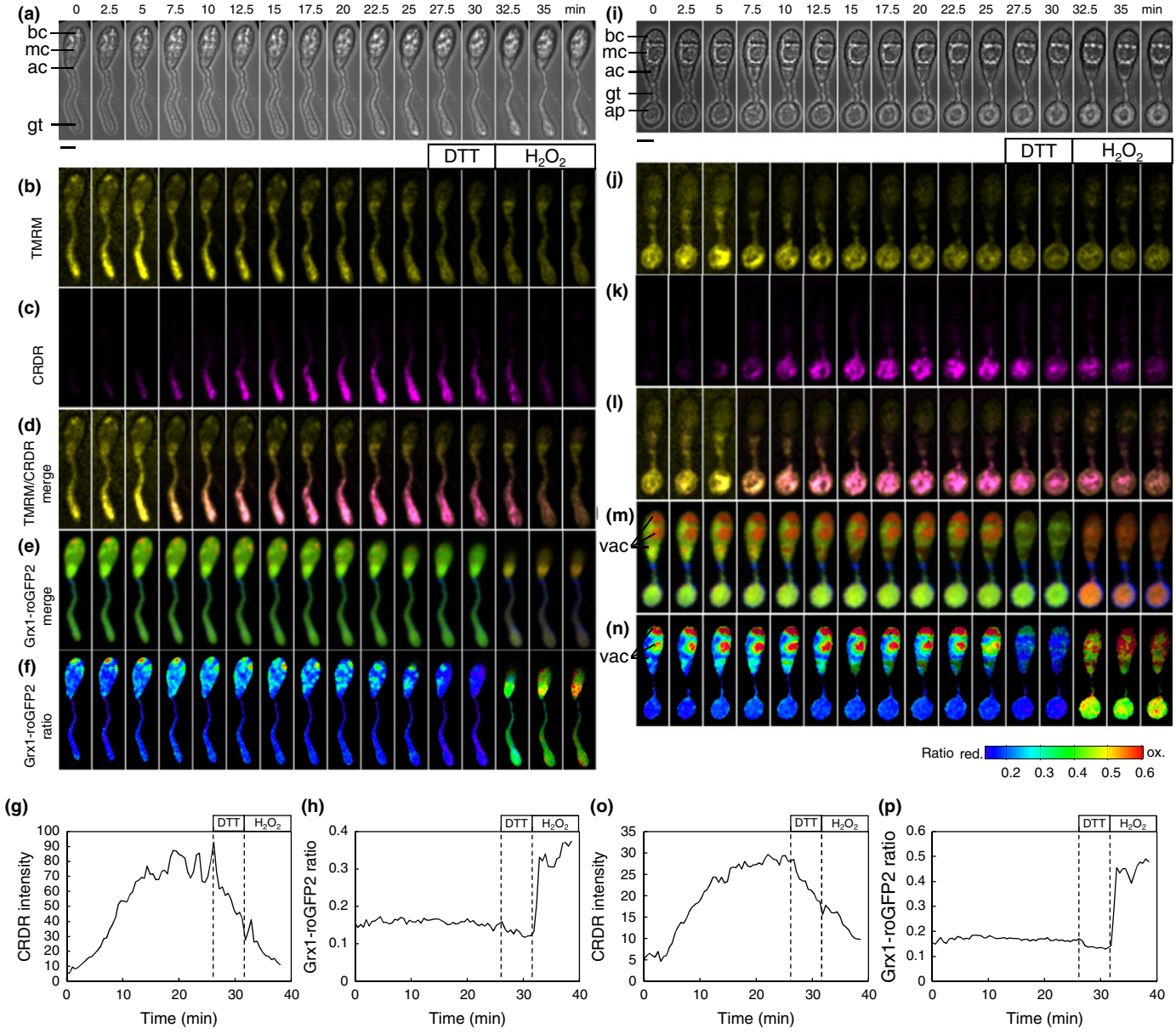

Fig. 4 Simultaneous measurement of reactive oxygen species (ROS), mitochondrial membrane potential and glutathione redox potential in germlings of *Magnaporthe oryzae*. Mitochondrial activity was measured using membrane potential partitioning of tetramethyl rhodamine methyl ester (TMRM) (excitation, 543 nm; emission, 561–603 nm) during germ tube growth (a, b) or appressorium formation (i, j). ROS were visualized in parallel with CellROX Deep Red (CRDR; excitation, 633 nm; emission, 657–721 nm) (c, k). Levels of ROS increased linearly in the cytoplasm of all three cells to a low level, but much more pronounced accumulation was observed in punctate structures in the apical cell and growing germ tube (b, g) or the appressorium (j,o). The punctate structures labelled by CRDR overlapped with the TMRM signal (d, l), from which we infer that CRDR predominantly reports mitochondrial ROS in this system. Cells also expressed Grx1-roGFP2, colour coded as Grx1-roGFP2$_{405}$ in red, Grx1-roGFP2$_{488}$ in green and autofluorescence in blue (e, m). The redox potential of the glutathione pool was measured simultaneously using ratio imaging (excitation, 405 nm, 488 nm; emission, 500–525 nm) following autofluorescence bleed-through correction (f, n), and showed a consistently reduced cytoplasmic redox potential during germ tube swelling (f, h) and appressorial formation (n, p). During the Grx1-roGFP2 calibration, the CRDR signal was also lost (g, o). Fluorescent images are shown as optimum plane projections of every fifth *z*-stack, following smoothing with a 3 × 3 × 3 spatial average, autofluorescence correction and low signal masking, from a multi-channel (*x*,*y*,*z*,*t*) four-dimensional image series collected at 30-s intervals. The bright-field image was a maximum brightness projection of the non-confocal transmission images collected in parallel. ac, apical cell; ap, appressorium; bc, basal cell; mc, mid cell; gt, germ tube. Bars, 5 μm. See Videos S3 and S4 for movies of the complete time series.

in autophagic cell death (Scherz-Shouval & Elazar, 2011), which forms part of the developmental programme in *M. oryzae* (Veneault-Fourrey *et al.*, 2006; Talbot & Kershaw, 2009).

TMRM labelling revealed highly motile tubular mitochondria, particularly in the apical cell during germ tube growth (Fig. 4b) and appressorium formation (Fig. 4j). In parallel, CRDR showed a time-dependent increase in punctate fluorescence in swelling germ tubes (Fig. 4c, see also Video S3) and developing appressoria (Fig. 4k, see also Video S4), which overlapped the TMRM signal (Fig. 4d,l). Lower levels of TMRM and CRDR

New Phytologist

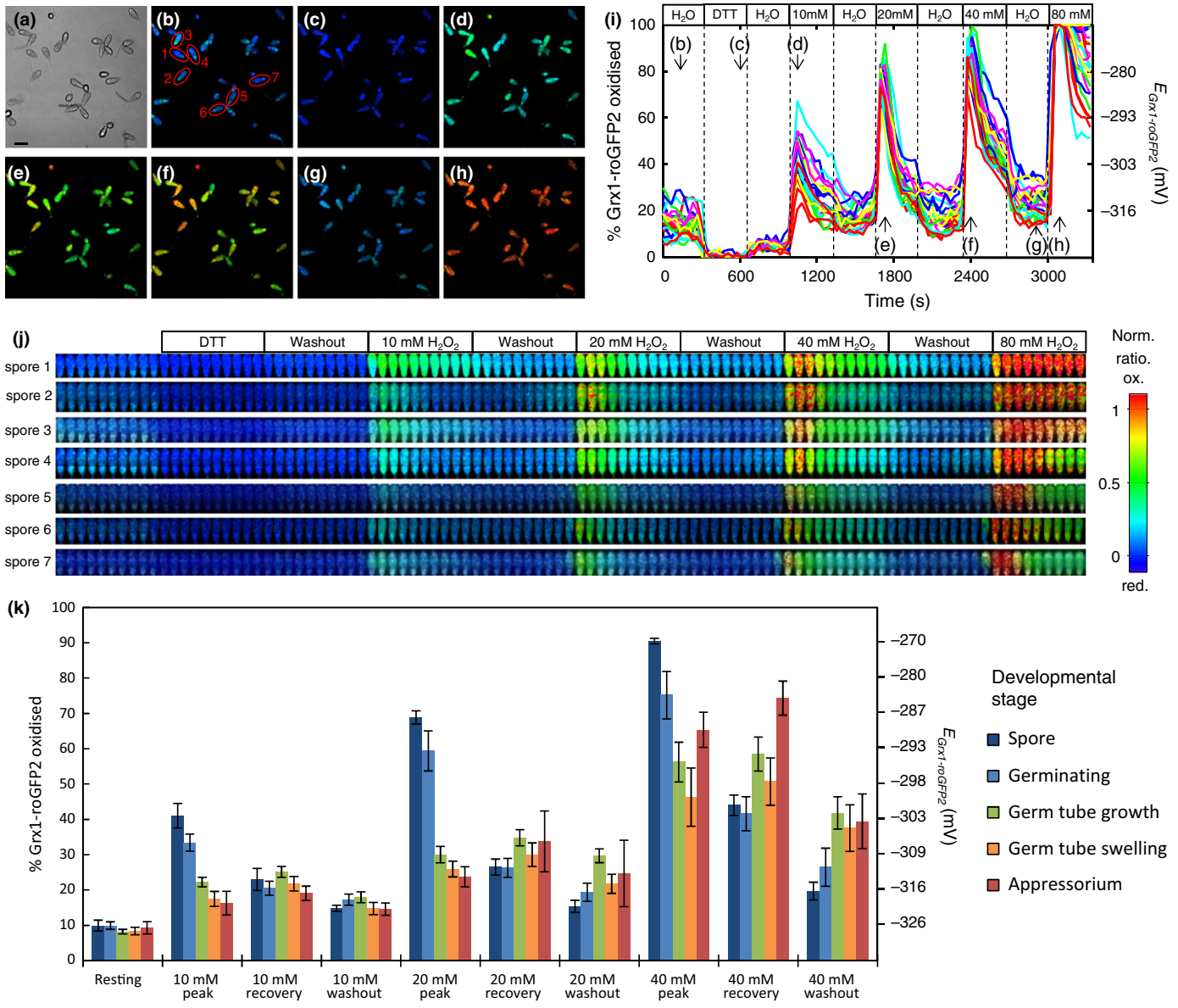

Fig. 5 Response of the redox potential of the glutathione pool to transient oxidative stress in germlings of *Magnaporthe oryzae*. The response to oxidative bursts was measured from the apical cell in populations of developing germlings at 2 h post-inoculation (hpi) (a) during transient exposure to increasing concentrations of H_2O_2. Cytoplasmic Grx1-roGFP2 was *c.* 10% oxidized in resting cells (b), although there was some variation between germlings (i), possibly reflecting the difficulty in unambiguously selecting cytoplasmic regions of interest in low magnification images. Dithiothreitol (DTT) was used initially to reduce the total glutathione pool and set the calibration minimum (c) and significantly reduced the variation in resting level after washout (i). A 5-min exposure to 10 mM H_2O_2 elicited strong transient oxidation of Grx1-roGFP2 to a peak at *c.* 35% (d), which recovered to a varying extent, even during continued exposure to H_2O_2 (i). Recovery was improved following washout of the H_2O_2 to *c.* 20% (i). The kinetics showed considerable variation between individual germlings in the duration of the response, and the extent of the recovery (i). A representative set of germling images, outlined in (b), is shown in (j), ordered with increasing tolerance to H_2O_2 shocks. Subsequent shocks with 20 mM (e) and 40 mM (f) gave more pronounced initial peaks, but the germlings were still able to recover to a considerable extent, even in the continued presence of H_2O_2 (i–k). Thus, following washout at the end of the pulse series (g), before the final calibration with 80 mM H_2O_2 (h), the level of Grx1-roGFP2 oxidation averaged *c.* 25%, or a shift in $E_{Grx1\text{-}roGFP2}$ from −326 to −312 mV for the experiment shown here (i–k). Germ tubes continued to grow following 10 and 20 mM shocks, but slowed or ceased to elongate at 40 mM and above. To determine whether there was any variation in response with development, germlings were grouped by developmental stage from five separate experiments and $OxD_{Grx1\text{-}roGFP2}$ was measured at the peak, recovery and washout phases during the pulse sequence (k). The corresponding values for $E_{Grx1\text{-}roGFP2}$, and hence E_{GSH}, are given assuming $E^{o\prime}_{Grx1\text{-}roGFP2} = -280$ mV and a cytoplasmic pH of pH 7.6. Both the initial peak and the recovery were most marked in spores and during germination, whereas transients in more advanced stages were less dramatic, but also showed less spontaneous recovery (k). Results are shown as mean ± SEM for: $n = 7$, spores; $n = 11$, germinating 1 hpi; $n = 36$, long germ tubes 2 hpi; $n = 24$, swollen germ tube 3 hpi; $n = 11$, appressorium 5 hpi. Bar, 20 μm.

accumulation were observed in the other cells throughout development (e.g. Fig. 4b–d,j–l, see also Fig. 3 h), even after extended periods of incubation. We infer that the mitochondria in these cells are in a different metabolic state, possibly geared towards the synthesis of metabolic intermediates (e.g. Patkar *et al.*, 2012a), rather than ATP production.

The Grx1-roGFP2 signal measured in parallel from the swelling germ tube apical tip (Fig. 4e,f,h, see also Video S3) and developing appressorium (Fig. 4m,n,p, see also Video S4) showed the expected reduced profile in the cytoplasm and a more oxidized signal in punctate vacuoles. However, there was no evidence for any substantial changes in $E_{Grx1\text{-}roGFP2}$ that might reflect a burst of ROS production (Fig. 4 h,p) during these and more than 30 other time series spanning 2–5 hpi when appressoria develop. Interestingly, the internal CRDR signal was also lost rapidly during the calibration sequence in these cells. We infer, as with DAR-4M and DCF, that CRDR can be rapidly expelled by *M. oryzae*.

The apparent compartmentalization of mitochondrial activity and ROS production was unexpected if the three cells of the spore have direct cytoplasmic continuity, as has been argued previously from transmission electron microscopy (TEM) images for *M. oryzae* conidia, which show open septal pores (Money & Howard, 1996; Soundararajan *et al.*, 2004). Equally, differential turgor pressures in adjacent cells have been interpreted as evidence for the regulation of pore opening and closure to permit the transfer of materials between cells (Money & Howard, 1996). We found evidence using fluorescence recovery after photobleaching (FRAP) of Grx1-roGFP2 that spore cells were functionally isolated during germination and hyphal growth, but allowed communication during appressorium formation (Fig. S1). Furthermore, TEM images (Methods S1) showed occlusion of some septal pores by Woronin bodies (Fig. S2). These data are consistent with regulated septal conductivity during early development, with an increased probability of opening when transfer of reserves to the developing appressorium is required.

It is clear that there are differential rates of endogenous ROS production in each cell of germlings of *M. oryzae* during early development. However, at this stage, we do not have strong evidence for oxidative shifts during developmental transitions from either ROS measurements or changes in $E_{Grx1\text{-}roGFP2}$. Equally, quantitative interpretation of ROS levels and localization are challenging, as the signal represents a dynamic balance between dye uptake, intracellular hydrolysis, ROS production, reaction rates and subsequent probe sequestration (Fricker *et al.*, 2001; Halliwell & Whiteman, 2004; Meyer & Fricker, 2008). It is also possible that the glutathione pool may not be the most sensitive marker for redox events involved in signalling (Patsoukis & Georgiou, 2004; Belozerskaya & Gessler, 2007; Winterbourn,

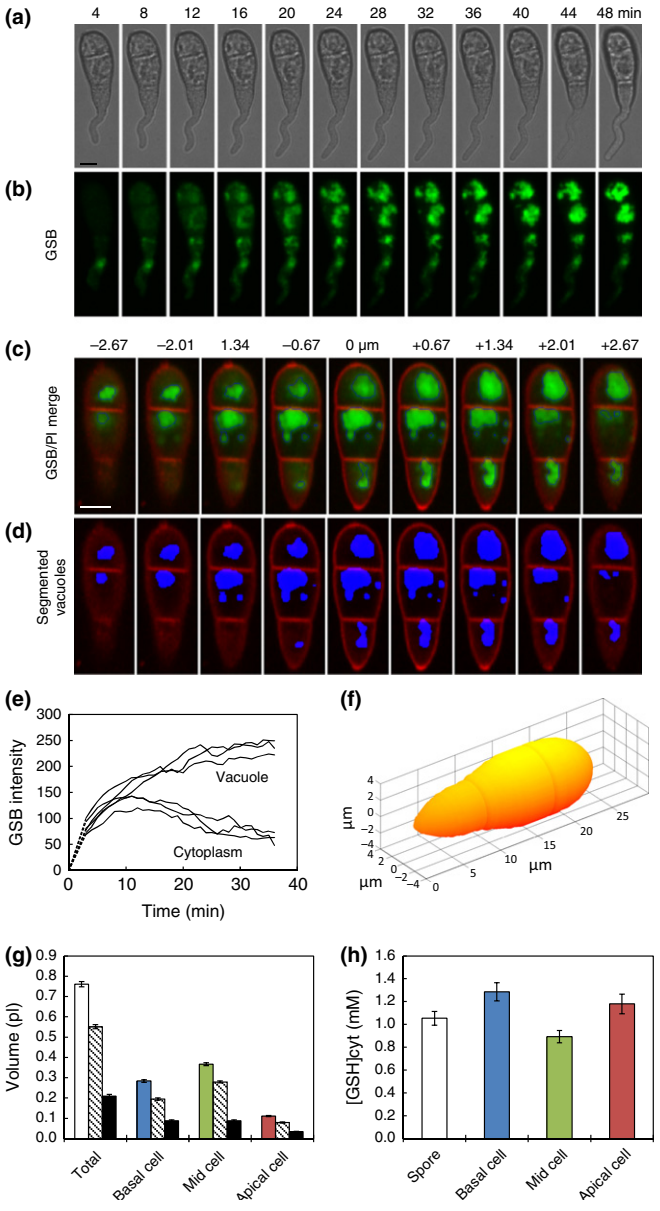

Fig. 6 Estimation of cytoplasmic GSH concentrations in *Magnaporthe oryzae* using *in vivo* imaging. Germinating spores of *M. oryzae* (a) were labelled with monochlorobimane (MCB), which reacts with GSH in the presence of a glutathione transferase to give fluorescent glutathione-bimane (GSB). GSB was imaged with four-dimensional (x,y,z,t) confocal microscopy (excitation, 405 nm; emission, 435–485 nm). The GSB signal increased in the cytoplasm during the initial reaction, but was transferred to the vacuole over time, possibly by a tonoplast GSX-conjugate pump. Maximum projections are shown in (b) for a subset of the time points in a typical experiment. Similar kinetics were observed from regions of interest from the basal, mid and germinating apical cell for both cytoplasmic and vacuolar areas (e). Labelling reached a plateau after *c.*30 min, with the majority of the signal in the vacuole. See Video S5 for a movie of the complete time series. The original cytoplasmic concentration of GSH was calculated from the total fluorescence in each compartment, corrected by the relative volume. To measure the total vacuolar volume and vacuolar GSB, individual vacuoles were separated using a three-dimensional watershed algorithm and then segmented using a local 50% intensity threshold above background for each vacuole (c, d). The total cell volume was calculated automatically from the outline of a maximum projection of the propidium iodide (PI)-stained cell wall, assuming that the spore was rotationally symmetric about the long axis (f). See Video S6 for example movies of the segmented vacuole images. The total spore volume was *c.* 0.76 ± 0.01 pl (mean ± SEM, $n = 81$), split in the ratio 37% : 48% : 15% basal : mid : apical (g). All three cells had a similar high cytoplasmic volume, *c.* 70% of the total cell volume (g) (open/coloured bars, total; hatched bars, cytoplasm; black bars, vacuole). The measured GSB intensities in the different compartments were calibrated against GSB standards, and the initial GSB cytoplasmic concentration was then calculated using the cytoplasmic and vacuolar volumes. The average was just over 1 mM (h), with slightly lower concentrations in the mid cell (h).

2008; Winterbourn & Hampton, 2008), with more reactive targets, such as thioredoxin and peroxiredoxins, being responsible for the initiation of developmental responses (D'Autreaux & Toledano, 2007; Meyer, 2008; Heller & Tudzynski, 2011). Indeed, it has been proposed in yeast that the primary function of cytosolic GSH is to drive extra-mitochondrial iron–sulfur cluster maturation, and GSH only acts as a back up to thioredoxin in redox homeostasis (Kumar *et al.*, 2011; Toledano *et al.*, 2013). The development of probes for these other redox couples is underway (Meyer & Dick, 2010) and would greatly facilitate physiological measurements in parallel with Grx1-roGFP2 to test such hypotheses. Likewise, the solution to understanding the spatial and temporal dynamics of ROS production would benefit from the further development of specific, transgenic ratio probes for the different ROS species, such as HyPer (Belousov *et al.*, 2006) or roGFP2-Orp1 (Gutscher *et al.*, 2009; Meyer & Dick, 2010).

M. oryzae can tolerate extreme oxidative stress

Whilst the maintenance of a highly reduced cytoplasm is required for normal cell physiology, one of the major defences in plants and animals to pathogen attack is through pronounced localized production of ROS to high levels, often within a few hours of inoculation (Xu *et al.*, 2009). We therefore tested how well *M. oryzae* might handle transient exposure to increasing concentrations of H_2O_2 to mimic attack by a host-derived oxidative burst.

In five extended time-series experiments, with a total of 89 germlings classified into different developmental stages, cells initially showed a rapid transient oxidation of Grx1-roGFP2 in response to short (5 min) exposure to increasing concentrations of H_2O_2, which returned to a more reduced state, even in the continued presence of the oxidant. A typical experiment is shown in Fig. 5 for a field of developing germlings (Fig. 5a). The average ratio for each apical cell is shown in Fig. 5(i). Ratio images are shown at low resolution for all cells at rest (Fig. 5b), following DTT (Fig. 5c), at the peak of each of the H_2O_2 exposures (Fig. 5d–f,h) and for the penultimate recovery (Fig. 5g). More detailed time-series images are shown for specific germlings to highlight the variability in response (Fig. 5j). Each increasing concentration of H_2O_2 gave a marked transient oxidation of Grx1-roGFP2 in these germlings, which rapidly returned towards resting levels, even in the continued presence of H_2O_2. The peak responses in other experiments were not as strong, but were captured in the average peak response for multiple cells and replicates (Fig. 5k). Washout of the H_2O_2 allowed $OxD_{Grx1\text{-}roGFP2}$ to return to near resting levels, even with treatments up to 40 mM H_2O_2 (Fig. 5i–k). Germ tube growth continued with 10 and 20 mM H_2O_2 shocks, but showed a reduction or ceased completely with 40–80 mM H_2O_2.

Within this overall pattern, there was variability in response at different developmental stages, most notably the rate of spontaneous recovery (Fig. 5i,j). During germination (0–1 hpi) and germ tube growth (2–3 hpi), the apical spore cell showed the greatest excursions in response to H_2O_2, but also the most rapid recovery (Fig. 5k). Developing appressoria (3–5 hpi) did not respond as strongly to oxidative stress, but also showed a lower subsequent rate of reduction of Grx1-roGFP2 (Fig. 5k). As noted previously, after *c.* 8 hpi, melanized appressoria were essentially insensitive to shocks of even 100 mM H_2O_2 (Fig. 2).

We infer that germlings of *M. oryzae* are able to withstand an aggressive imposed oxidative burst of H_2O_2, with transient excursions rapidly brought down to a new steady state. Germ tube growth continued in short-term exposures to 10–20 mM H_2O_2, whilst the melanizing appressorium was impervious to much higher H_2O_2 concentrations. The difference in $E^{o'pH}_{Grx1-roGFP2}$ and $E^{o'pH}_{GSH}$ makes Grx1-roGFP2 particularly sensitive to subtle shifts in E_{GSH}, with submicromolar cytoplasmic concentrations of GSSG, even with millimolar concentrations of exogenous H_2O_2. In addition to the rapid reduction of GSSG by glutathione reductase, it is possible that GSSG is sequestered in the vacuole to maintain tight control of cytoplasmic E_{GSH}, as has recently been documented for yeast (Morgan *et al.*, 2013).

Fig. 7 Redox relationships during infection of susceptible CO39 rice leaf sheaths with *Magnaporthe oryzae* expressing Grx1-roGFP2. Spores expressing Grx1-roGFP2 were inoculated on rice cultivar CO39 and three-dimensional (*x,y,z*) images were collected with dual-excitation confocal ratio imaging of Grx1-roGFP2 with excitation at 405 nm (c, i, o, s) or 488 nm (d, j, p, t) and emission at 500–530 nm, and additional wall autofluorescence (with either excitation at 405 nm, emission at 435–485 nm or excitation at 543 nm, emission at 656–615 nm). Bright-field images (a, g, m) were collected in parallel with a non-confocal transmission detector. Fluorescence channels were merged and colour coded as $Grx1\text{-}roGFP2_{405}$ in red, $Grx1\text{-}roGFP2_{488}$ in green and autofluorescence in blue (b, h, n, v), particularly to map the level of oxidative host response, visible as a red/purple colour in the cell walls. *In situ* calibration was not possible, but occasionally dying hyphae with oxidized Grx1-roGFP2 were observed (a–e). The ratio image (e) and pixel population statistics, fitted with a two-component Gaussian mixture model (GMM), confirmed that the dynamic range of the probe measured during infection was comparable with that observed for spores germinated on coverslips and imaged in parallel (f). During the early stages of infection, *c.* 16 h post-inoculation (hpi) (g), Grx1-roGFP2 signals from the cytoplasm in the appressorium (ap) and invasion hyphae (ih), and vacuoles (vac) in the appressorium and apical cell (ac) could be distinguished (h–j), and reported different degrees of oxidation in the ratio image (k) and population statistics, fitted with a four-component GMM (l). At 24 hpi (m), the majority of the signal could be attributed to cytoplasmic Grx1-roGFP2 in the invasion hyphae (n–p), although there was some host wall fluorescence arising from the host response with a very different broad spectrum (n, q). Cytoplasmic Grx1-roGFP2 was highly reduced in both the appressorium and invasion hyphae (q), and clearly separated from the autofluorescence in the pixel distributions (r). By 48 hpi, microscopic lesions were beginning to form as hyphae spread to multiple adjacent cells (s–w). Levels of vacuolation increased, particularly in the centre of the colony (v and w), but the cytoplasmic and vacuolar Grx1-roGFP2 signals were well separated using a two-component GMM (u). Two-component GMM models were also fitted to the cytoplasm and vacuoles in the centre and periphery of the colony separately, which showed a very slight increase in $E_{Grx1\text{-}roGFP2}$, but a more substantial increase in the vacuoles (x, mean ± SEM, $n = 17$). Images are presented as optimum plane projections of three-dimensional (*x,y,z*) stacks collected at 3-μm intervals. bc, basal cell; cyt, cytoplasm; gt, germ tube; mc, mid cell; sp, spore. Bars, 10 μm. See Video S7 for movies of 16- and 24-hpi time points, and Video S8 for the 48-hpi time point.

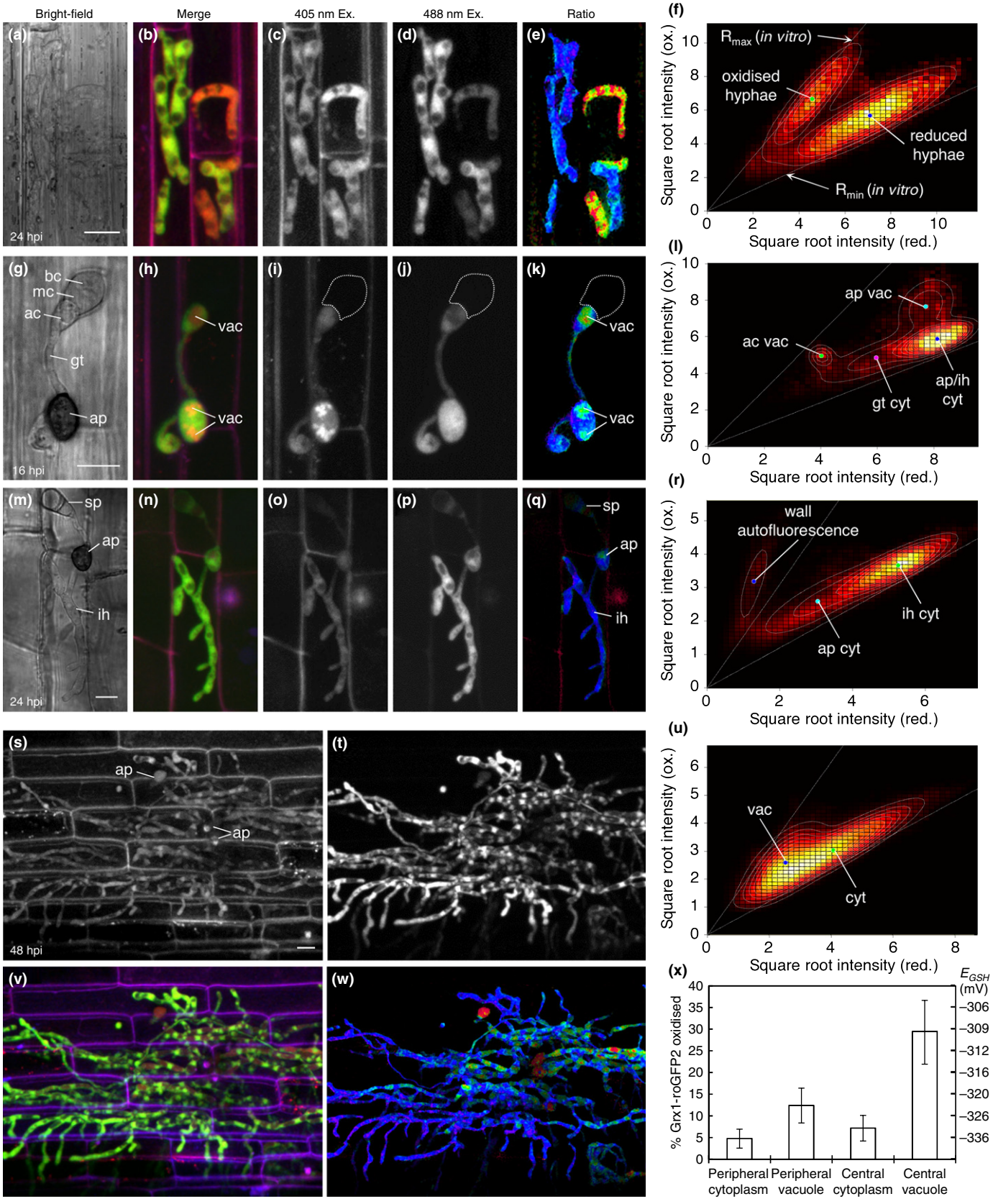

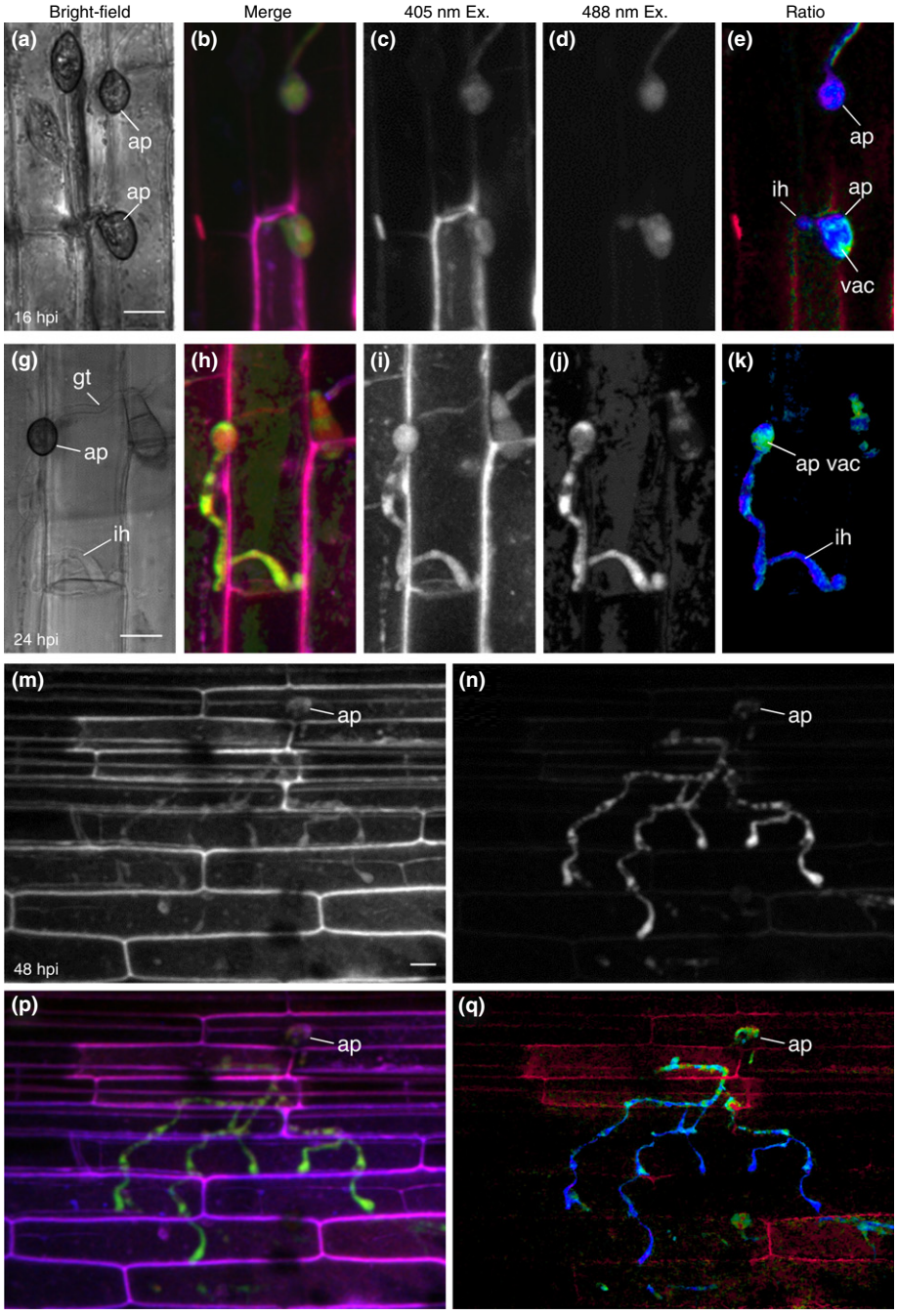

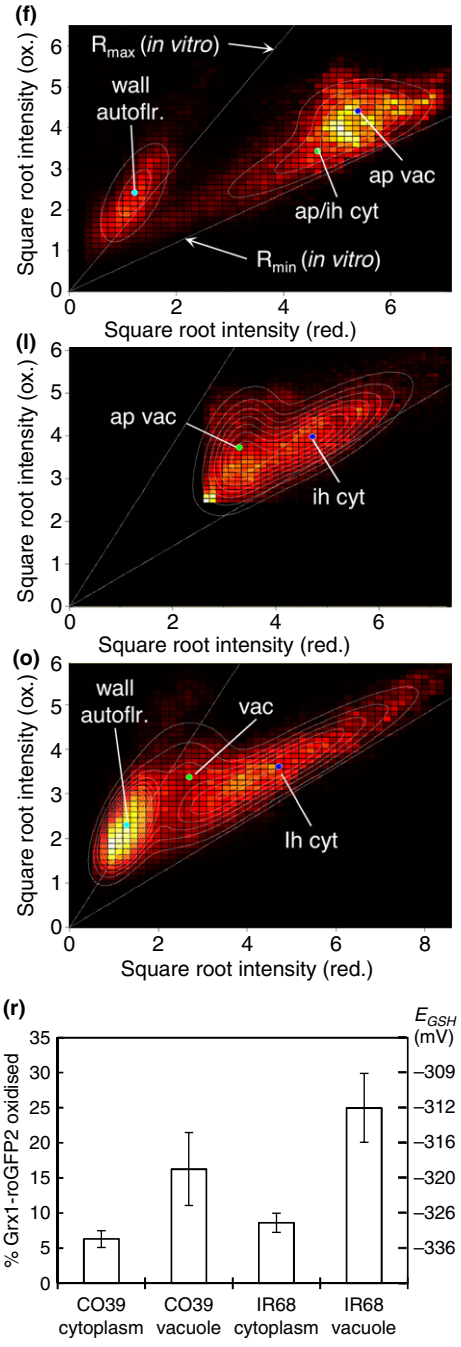

Fig. 8 Redox relationships during infection of resistant IR68 rice leaf sheaths with *Magnaporthe oryzae* expressing Grx1-roGFP2. The majority of spores failed to form penetration pegs on the resistant IR68 rice variety. However, occasionally successful penetration was observed followed by limited intracellular development. At 16 h post-inoculation (hpi) (a), there was considerable wall autofluorescence in infected cells, particularly with excitation at 405 nm (b–d), although the Grx1-roGFP2 signal remained reduced in the appressorium and invasion hyphae (e). Bright-field images (a, g) were collected in parallel with a non-confocal transmission detector. Fluorescence channels were merged and colour coded as Grx1-roGFP2$_{405}$ in red, Grx1-roGFP2$_{488}$ in green and autofluorescence in blue (b, h, p), particularly to map the level of the oxidative host response, visible as a red/purple colour in the cell walls. It was possible to separate out the wall autofluorescence and cytoplasmic and vacuolar signals with a three-component Gaussian mixture model (GMM) (f). At 24 hpi, rare intracellular growth was observed, with relatively thin, un-branched and vacuolated hyphae (g) and considerable localized wall autofluorescence, particularly with excitation at 405 nm (h–j). Cytoplasmic Grx1-roGFP remained fully reduced (k, l). At 48 hpi, there was occasional spindly growth through multiple cells with little or no branching (m–q). Fluorescent signals were relatively weak (m, n) and there were high levels of wall autofluorescence (p). Nevertheless, the ratio still showed a reduced signal through much of the cytoplasm (q). A three-component GMM fitted to the pixel distributions confirmed that cytoplasmic Grx1-roGFP2 remained reduced (o), and comparisons showed that the degree of cytoplasmic oxidation was only marginally higher in the resistant IR68 (mean ± SEM, $n = 10$) than in the susceptible CO39 (mean ± SEM, $n = 17$) cultivar (r). Images are presented as optimum plane projections of three-dimensional (x,y,z) stacks collected at 3-μm intervals. ap, appressorium; cyt, cytoplasm; ih, invasion hyphae; vac, vacuole. Bars, 10 μm. See Video S9 for a movie of 16- and 24-hpi time points, and Video S10 for the 48-hpi time point.

GSH levels are at millimolar concentrations in *M. oryzae*

Given the variable levels of endogenous ROS observed, the highly reduced E_{GSH} and the ability to tolerate substantial external bursts of H_2O_2, we sought to measure the absolute cytoplasmic concentration of glutathione to determine whether *M. oryzae* has a particularly high anti-oxidant capacity compared with non-pathogenic fungi and other organisms. Total levels of GSH were measured following *in situ* reaction with MCB to give a fluorescent GSB conjugate (Fricker *et al.*, 2000; Meyer & Fricker, 2000, 2008; Fricker & Meyer, 2001; Meyer *et al.*, 2001). MCB requires a glutathione transferase to react at an appreciable rate *in vivo*, and thus preferentially labels the existing cytoplasmic GSH pool, together with any GSSG that can be re-reduced by glutathione reductase (Fricker *et al.*, 2000; Meyer & Fricker, 2000; Fricker & Meyer, 2001; Meyer *et al.*, 2001). GSB was formed in the cytoplasm initially, and subsequently sequestered in the vacuoles over *c.* 30 min (Fig. 6a,b, see also Video S5), with similar kinetics in all three cells of the spore (Fig. 6e). This matches the xenobiotic detoxification pathways in plant and animal systems, where GSB is exported from the cytoplasm by glutathione-S-conjugate pumps (Coleman *et al.*, 1997; Fricker & Meyer, 2001). To measure the original cytoplasmic GSH concentration, the total GSB was corrected for the relative volume of the cytoplasmic and vacuolar compartments. The volume of the numerous vacuoles was determined from segmentation of the bimane images (Fig. 6c,d, see also Video S6), whereas the total cell volume was estimated from a maximum projection of the PI-stained cell wall, assuming that the spore was rotationally symmetric about the long axis (Fig. 6f). The cytoplasmic volume was calculated as the difference between the total cell and vacuolar volumes (Fig. 6g). At this stage of development, all three cells in the spore were densely cytoplasmic, at *c.* 70% of the total cell volume. Using the estimated cytoplasmic and vacuolar volumes, the total GSH concentration ranged from 1.29 ± 0.08 mM in the basal cell to 0.89 ± 0.05 mM in the mid cell, $n = 81$ (Fig. 6 h).

These GSH concentrations are comparable with those of aerial plant tissues, but at the low end for root tissues, yeast and mammalian cells (Meister & Anderson, 1983; Meyer, 2008; Noctor *et al.*, 2012). Thus, it appears that anti-oxidant defences in *M. oryzae* are not based on a massive constitutive GSH pool; the highly reduced E_{GSH} must be based on either rapid re-reduction of any GSSG produced or rapid removal of GSSG, or both (Morgan *et al.*, 2013).

M. oryzae does not appear to experience oxidative stress *in vivo*

Having determined the amount of GSH, and the capacity of *M. oryzae* to withstand imposed oxidative stress, we asked what happens to E_{GSH} during infection. On susceptible hosts, *M. oryzae* formed appressoria and penetration pegs within 16 hpi (Fig. 7g, see also Video S7), which developed to form swollen, branched infection hyphae by 24 hpi (Fig. 7m, see also Video S7). Over the next 24 h, *M. oryzae* colonized and spread through neighbouring cells to form small, microscopic lesions by 48 hpi (Fig. 7s, see also Video S8).

The quantification of E_{GSH} in hyphae ramifying in three dimensions was challenging, as single-point measurements did not capture the potential variation throughout the colony. Estimates were further complicated by vacuolar Grx1-roGFP2 signals, and high levels of host autofluorescence. Thus, we developed a pixel population approach to quantify $OxD_{Grx1\text{-}roGFP2}$ within the entire network structure. The fluorescence signal at both excitation wavelengths of Grx1-roGFP2 was fitted with a Gaussian mixture model (GMM) comprising two to four components (Fig. 7f,l,r,u), reflecting different cytoplasmic, vacuolar or autofluorescence signals in different regions of the colony. Ratios were compared with *in situ* calibration of germinating spores imaged under the same conditions. It was not possible to perform a comparable *in planta* calibration, because of the strong reaction of the plant tissue to the high H_2O_2 concentrations needed to calibrate Grx1-roGFP2 within intracellular fungal hyphae (data not shown). Occasionally, however, cells containing dying hyphae were observed, which provided an internal control for oxidized Grx1-roGFP2 (Fig. 7a–f), and confirmed the applicability of the *ex planta* calibration.

Cytoplasmic E_{GSH} was highly reduced throughout the infection process when quantified by ratio imaging (Fig. 7k,q,w, see also Videos S7, S8) or Gaussian modelling (Fig. 7 l,r,u). Both approaches highlighted the more oxidized signal from the numerous vacuoles present, particularly at later stages of infection (Fig. 7w). There were increasing levels of host wall fluorescence visible as a red/purple colour, resulting from the overlap between the autofluorescence channel, coded in blue, and bleed-through into the $GRx1\text{-}roGFP2_{405}$ channel, coded in red (Fig. 7h,n,v), indicative of a host ROS response. Around 48 hpi, the centre of the lesion showed some cell necrosis (Fig. 7v,w), a slightly higher average cytoplasmic redox potential compared with hyphae from the expanding colony margin, and an increased number of vacuoles with oxidized Grx1-roGFP2 (Fig. 7x). In general, Grx1-roGFP2 reported a highly reduced E_{GSH} throughout, with no evidence for shifts during early penetration events at *c.* 16–24 hpi, or during subsequent internal colonization.

In a resistant IR68 cultivar, cell penetration and intracellular development of *M. oryzae* were dramatically reduced with few successful penetration events and much higher levels of host wall autofluorescence or cell death, consistent with a strong oxidative host defence response (Fig. 8b,h,p, see also Videos S9, S10). Nevertheless, spores, germ tubes and the numerous appressoria unable to form infection pegs still maintained a reduced cytoplasmic GSH pool (see upper appressorium in Fig. 8e), with no evidence for extensive oxidation of Grx1-roGFP2 in the ratio images (Fig. 8e, see also Videos S9, S10) or GMM (Fig. 8f). When sparse intracellular hyphae did form, they were thinner than in the susceptible interaction, more vacuolated, and appeared to migrate between cells with little or no intracellular branching (Fig. 8 h,p). Nevertheless, the cytoplasmic E_{GSH} of these hyphae remained as highly reduced as in the susceptible plants (Fig. 8e,k,i,q, see also Videos S9, S10).

This represents something of a conundrum – at a physiological level, it is not obvious that ROS toxicity plays a dominant role in host resistance to rice blast as, under normal circumstances, *M. oryzae* has sufficient anti-oxidant defences to deal with both endogenous and exogenous ROS production and tightly regulates E_{GSH} with submicromolar levels of oxidized GSSG present. Equally, fungal mutants that have compromised anti-oxidant pathways suffer decreased pathogenicity. This parallels the results reported for the necrotroph *B. cinerea* (Temme & Tudzynski, 2009), in which the key redox-sensitive regulatory transcription factor, Bap1, was required for tolerance to exogenous H_2O_2 *ex planta*, but the corresponding Bap1 target genes were not induced during infection, with the clear implication that the fungus was not experiencing oxidative stress *in planta*. Furthermore, Bap1 was not essential for pathogenesis (Temme & Tudzynski, 2009), similar to results for the deletion of AP1 homologues in the human pathogen *Aspergillus fumigatus* (Lessing *et al.*, 2007) and the plant pathogen *Cochliobolus heterotrophus* (Lev *et al.*, 2005). The situation in *M. oryzae* is not identical, as deletion of the homologous gene, *MoAP1*, causes a reduction in pathogenicity, but during later intracellular infection and hyphal growth, rather than during appressorium formation and host penetration. MoAP1 has a wide range of targets, but reduced secretion of peroxidases and laccases might provide the strongest mechanistic link to ROS tolerance (Guo *et al.*, 2010, 2011). Similarly, deletion of *AP1* homologues in *Ustilago maydis* (Molina & Kahmann, 2007) and *Alternaria alternata* (Lin *et al.*, 2009, 2011; Yang *et al.*, 2009) also affects both H_2O_2 tolerance and pathogenicity.

The overall picture emerging is that *M. oryzae* tightly regulates E_{GSH} and has sufficient anti-oxidant capacity to handle even a strong host response, with the consequence that ROS toxicity alone is not sufficient to kill the pathogen. We infer that a distinction needs to be drawn between the presence of a high oxidative load during the host response, and the extent that a fungus actually experiences oxidative stress *in planta*, which cannot necessarily be inferred from *ex planta* responses to oxidative stress, but requires *in vivo* measurements.

Acknowledgements

Funding was provided by the Biotechnology and Biological Sciences Research Council (BBSRC) (BB/G00207X/1) to S.J.G. and M.D.F. We would like to thank Sarah Rodgers for the TEM images and Ian Moore for reading the manuscript.

References

Aguirre J, Lambeth JD. 2010. Nox enzymes from fungus to fly to fish and what they tell us about Nox function in mammals. *Free Radical Biology and Medicine* **49**: 1342–1353.

Aguirre J, Rios-Momberg M, Hewitt D, Hansberg W. 2005. Reactive oxygen species and development in microbial eukaryotes. *Trends in Microbiology* **13**: 111–118.

Ausubel FM, Brent R, Kingston RE, Moore DD, Seidman JG, Smith JA, Struhl K. 1999. *Short protocols in molecular biology: a compendium of methods from current protocols in molecular biology.* Chichester, UK: John Wiley.

Belousov VV, Fradkov AF, Lukyanov KA, Staroverov DB, Shakhbazov KS, Terskikh AV, Lukyanov S. 2006. Genetically encoded fluorescent indicator for intracellular hydrogen peroxide. *Nature Methods* **3**: 281–286.

Belozerskaya TA, Gessler NN. 2007. Reactive oxygen species and the strategy of antioxidant defense in fungi: a review. *Applied Biochemistry and Microbiology* **43**: 506–515.

Bolwell GP, Bindschedler LV, Blee KA, Butt VS, Davies DR, Gardner SL, Gerrish C, Minibayeva F. 2002. The apoplastic oxidative burst in response to biotic stress in plants: a three-component system. *Journal of Experimental Botany* **53**: 1367–1376.

Chi M-H, Park S-Y, Kim S, Lee Y-H. 2009. A novel pathogenicity gene is required in the rice blast fungus to suppress the basal defenses of the host. *PLoS Pathogens* **5**: e1000401.

Coleman JJ, Mylonakis E. 2009. Efflux in fungi: la piece de resistance. *PLoS Pathogens* **5**: e1000486.

Coleman JOD, BlakeKalff MMA, Davies TGE. 1997. Detoxification of xenobiotics by plants: chemical modification and vacuolar compartmentation. *Trends in Plant Science* **2**: 144–151.

Czymmek KJ, Bourett TM, Sweigard JA, Carroll A, Howard RJ. 2002. Utility of cytoplasmic fluorescent proteins for live-cell imaging of *Magnaporthe grisea* in planta. *Mycologia* **94**: 280–289.

D'Autreaux B, Toledano MB. 2007. ROS as signalling molecules: mechanisms that generate specificity in ROS homeostasis. *Nature Reviews in Molecular and Cellular Biology* **8**: 813–824.

Dean RA, Talbot NJ, Ebbole DJ, Farman ML, Mitchell TK, Orbach MJ, Thon M, Kulkarni R, Xu JR, Pan HQ *et al.* 2005. The genome sequence of the rice blast fungus *Magnaporthe grisea*. *Nature (London)* **434**: 980–986.

Dooley CT, Dore TM, Hanson GT, Jackson WC, Remington SJ, Tsien RY. 2004. Imaging dynamic redox changes in mammalian cells with green fluorescent protein indicators. *Journal of Biological Chemistry* **279**: 22284–22293.

Egan MJ, Talbot NJ. 2008. Genomes, free radicals and plant cell invasion: recent developments in plant pathogenic fungi. *Current Opinion in Plant Biology* **11**: 367–372.

Egan MJ, Wang ZY, Jones MA, Smirnoff N, Talbot NJ. 2007. Generation of reactive oxygen species by fungal NADPH oxidases is required for rice blast disease. *Proceedings of the National Academy of Sciences, USA* **104**: 11772–11777.

van Engelen FA, Molthoff JW, Conner AJ, Nap JP, Pereira A, Stiekema WJ. 1995. pBINPLUS: an improved plant transformation vector based on pBIN19. *Transgenic Research* **4**: 288–290.

Errington RJ, Fricker MD, Wood JL, Hall AC, White NS. 1997. Four-dimensional imaging of living chondrocytes in cartilage using confocal microscopy: a pragmatic approach. *American Journal of Physiology-Cell Physiology* **41**: C1040–C1051.

Fisher MC, Henk DA, Briggs CJ, Brownstein JS, Madoff LC, McCraw SL, Gurr SJ. 2012. Emerging fungal threats to animal, plant and ecosystem health. *Nature (London)* **484**: 186–194.

Fricker MD, May M, Meyer AJ, Sheard N, White NS. 2000. Measurement of glutathione levels in intact roots of *Arabidopsis*. *Journal of Microscopy* **198**: 162–173.

Fricker MD, Meyer AJ. 2001. Confocal imaging of metabolism *in vivo*: pitfalls and possibilities. *Journal of Experimental Botany* **52**: 631–640.

Fricker MD, Parsons A, Tlalka M, Blancaflor E, Gilroy S, Meyer A, Plieth C. 2001. Fluorescent probes for living plant cells. In: Hawes C, Satiat-Jeunemaitre B, eds. *Plant cell biology: a practical approach.* Oxford, UK: OUP, 35–84.

Georgiou CD, Petropoulou KP. 2001. Role of erythroascorbate and ascorbate in sclerotial differentiation in *Sclerotinia sclerotiorum*. *Mycological Research* **105**: 1364–1370.

Gessler NN, Aver'yanov AA, Belozerskaya TA. 2007. Reactive oxygen species in regulation of fungal development. *Biochemistry-Moscow* **72**: 1091–1109.

Gilbert MJ, Thornton CR, Wakley GE, Talbot NJ. 2006. A P-type ATPase required for rice blast disease and induction of host resistance. *Nature (London)* **440**: 535–539.

Govrin EM, Levine A. 2000. The hypersensitive response facilitates plant infection by the necrotrophic pathogen Botrytis cinerea. *Current Biology* **10**: 751–757.

Guo M, Chen Y, Du Y, Dong YH, Guo W, Zhai S, Zhang HF, Dong SM, Zhang ZG, Wang YC *et al.* 2011. The bZIP transcription factor MoAP1 mediates the oxidative stress response and is critical for pathogenicity of the rice blast fungus *Magnaporthe oryzae*. *PLoS Pathogens* **7**: e1001302.

Guo M, Guo W, Chen Y, Dong S, Zhang X, Zhang H, Song W, Wang W, Wang Q, Lv R *et al.* 2010. The basic leucine zipper transcription factor Moatf1 mediates oxidative stress responses and is necessary for full virulence of the rice blast fungus *Magnaporthe oryzae*. *Molecular Plant–Microbe Interactions* **23**: 1053–1068.

Gutscher M, Pauleau AL, Marty L, Brach T, Wabnitz GH, Samstag Y, Meyer AJ, Dick TP. 2008. Real-time imaging of the intracellular glutathione redox potential. *Nature Methods* **5**: 553–559.

Gutscher M, Sobotta MC, Wabnitz GH, Ballikaya S, Meyer AJ, Samstag Y, Dick TP. 2009. Proximity-based protein thiol oxidation by H_2O_2-scavenging peroxidases. *Journal of Biological Chemistry* **284**: 31532–31540.

Halliwell B, Whiteman M. 2004. Measuring reactive species and oxidative damage *in vivo* and in cell culture: how should you do it and what do the results mean? *British Journal of Pharmacology* **142**: 231–255.

Hansberg W, Aguirre J. 1990. Hyperoxidant states cause microbial cell-differentiation by cell isolation from dioxygen. *Journal of Theoretical Biology* **142**: 201–221.

Hanson GT, Aggeler R, Oglesbee D, Cannon M, Capaldi RA, Tsien RY, Remington SJ. 2004. Investigating mitochondrial redox potential with redox-sensitive green fluorescent protein indicators. *Journal of Biological Chemistry* **279**: 13044–13053.

Heller J, Meyer AJ, Tudzynski P. 2012. Redox-sensitive GFP2: use of the genetically encoded biosensor of the redox status in the filamentous fungus *Botrytis cinerea*. *Molecular Plant Pathology* **13**: 935–947.

Heller J, Tudzynski P. 2011. Reactive oxygen species in phytopathogenic fungi: signaling, development, and disease. *Annual Review of Phytopathology* **49**: 369–390.

Hesse SJA, Ruijter GJG, Dijkema C, Visser J. 2002. Intracellular pH homeostasis in the filamentous fungus *Aspergillus niger*. *European Journal of Biochemistry* **269**: 3485–3494.

Howard RJ, Ferrari MA, Roach DH, Money NP. 1991. Penetration of hard substrates by a fungus employing enormous turgor pressures. *Proceedings of the National Academy of Sciences, USA* **88**: 11281–11284.

Huang K, Czymmek KJ, Caplan JL, Sweigard JA, Donofrio NM. 2011. HYR1-mediated detoxification of reactive oxygen species is required for full virulence in the rice blast fungus. *PLoS Pathogens* **7**: e1001335.

Hubbart S, Peng S, Horton P, Chen Y, Murchie EH. 2007. Trends in leaf photosynthesis in historical rice varieties developed in the Philippines since 1966. *Journal of Experimental Botany* **58**: 3429–3438.

Kankanala P, Czymmek K, Valent B. 2007. Roles for rice membrane dynamics and plasmodesmata during biotrophic invasion by the blast fungus. *Plant Cell* **19**: 706–724.

Kim K-H, Willger SD, Park S-W, Puttikamonkul S, Grahl N, Cho Y, Mukhopadhyay B, Cramer RA Jr, Lawrence CB. 2009. TmpL, a transmembrane protein required for intracellular redox homeostasis and virulence in a plant and an animal fungal pathogen. *Plos Pathogens* **5**: e1000653.

Kumar C, Igbaria A, D'Autreaux B, Planson AG, Junot C, Godat E, Bachhawat AK, Delaunay-Moisan A, Toledano MB. 2011. Glutathione revisited: a vital function in iron metabolism and ancillary role in thiol-redox control. *EMBO Journal* **30**: 2044–2056.

Lamb C, Dixon RA. 1997. The oxidative burst in plant disease resistance. *Annual Review of Plant Physiology and Plant Molecular Biology* **48**: 251–275.

Lessing F, Kniemeyer O, Wozniok I, Loeffler J, Kurzai O, Haertl A, Brakhage AA. 2007. The *Aspergillus fumigatus* transcriptional regulator AfYap1 represents the major regulator for defense against reactive oxygen intermediates but is dispensable for pathogenicity in an intranasal mouse infection model. *Eukaryotic Cell* **6**: 2290–2302.

Lev S, Hadar R, Amedeo P, Baker SE, Yoder OC, Horwitz BA. 2005. Activation of an AP1-like transcription factor of the maize pathogen *Cochliobolus heterostrophus* in response to oxidative stress and plant signals. *Eukaryotic Cell* **4**: 443–454.

Levine A, Tenhaken R, Dixon R, Lamb C. 1994. H_2O_2 from the oxidative burst orchestrates the plant hypersensitive disease resistance response. *Cell* **79**: 583–593.

Lin CH, Yang SL, Chung KR. 2009. The YAP1 homolog-mediated oxidative stress tolerance is crucial for pathogenicity of the necrotrophic fungus *Alternaria alternata* in citrus. *Molecular Plant–Microbe Interactions* **22**: 942–952.

Lin C-H, Yang SL, Chung K-R. 2011. Cellular responses required for oxidative stress tolerance, colonization, and lesion formation by the necrotrophic fungus *Alternaria alternata* in citrus. *Current Microbiology* **62**: 807–815.

Marino D, Dunand C, Puppo A, Pauly N. 2012. A burst of plant NADPH oxidases. *Trends in Plant Science* **17**: 9–15.

Mathioni SM, Belo A, Rizzo CJ, Dean RA, Donofrio NM. 2011. Transcriptome profiling of the rice blast fungus during invasive plant infection and *in vitro* stresses. *BMC Genomics* **12**: 49.

Meister A, Anderson ME. 1983. Glutathione. *Annual Review of Biochemistry* **52**: 711–760.

Meyer AJ. 2008. The integration of glutathione homeostasis and redox signaling. *Journal of Plant Physiology* **165**: 1390–1403.

Meyer AJ, Dick TP. 2010. Fluorescent protein-based redox probes. *Antioxidants & Redox Signaling* **13**: 621–650.

Meyer AJ, Fricker MD. 2000. Direct measurement of glutathione in epidermal cells of intact *Arabidopsis* roots by two-photon laser scanning microscopy. *Journal of Microscopy-Oxford* **198**: 174–181.

Meyer AJ, Fricker MD. 2002. Control of demand-driven biosynthesis of glutathione in green *Arabidopsis* suspension culture cells. *Plant Physiology* **130**: 1927–1937.

Meyer AJ, Fricker MD 2008. Imaging thiol-based redox processes in live cells. In: Hell R, Dahl C, Knaff D, Leustek T, eds. *Sulfur metabolism in phototrophic organism. Advances in photosynthesis and respiration, vol 27*. Dordrecht, Netherlands: Springer, 483–501.

Meyer AJ, May MJ, Fricker M. 2001. Quantitative *in vivo* measurement of glutathione in *Arabidopsis* cells. *Plant Journal* **27**: 67–78.

Molina L, Kahmann R. 2007. An *Ustilago maydis* gene involved in H_2O_2 detoxification is required for virulence. *Plant Cell* **19**: 2293–2309.

Money NP, Howard RJ. 1996. Confirmation of a link between fungal pigmentation, turgor pressure, and pathogenicity using a new method of turgor measurement. *Fungal Genetics and Biology* **20**: 217–227.

Morel M, Kohler A, Martin F, Gelhaye E, Rouhier N. 2008. Comparison of the thiol-dependent antioxidant systems in the ectomycorrhizal *Laccaria bicolor* and the saprotrophic *Phanerochaete chrysosporium*. *New Phytologist* **180**: 391–407.

Morgan B, Ezeriņa D, Amoako TNE, Riemer J, Seedorf M, Dick TP. 2013. Multiple glutathione disulfide removal pathways mediate cytosolic redox homeostasis. *Nature Chemical Biology* **9**: 119–125.

Morgan B, Sobotta MC, Dick TP. 2011. Measuring EGSH and H_2O_2 with roGFP2-based redox probes. *Free Radical Biology and Medicine* **51**: 1943–1951.

Mur LAJ, Kenton P, Lloyd AJ, Ougham H, Prats E. 2008. The hypersensitive response; the centenary is upon us but how much do we know? *Journal of Experimental Botany* **59**: 501–520.

Noctor G, Mhamdi A, Chaouch S, Han Y, Neukermans J, Marquez-Garcia B, Queval G, Foyer CH. 2012. Glutathione in plants: an integrated overview. *Plant, Cell & Environment* **35**: 454–484.

Oh Y, Donofrio N, Pan HQ, Coughlan S, Brown DE, Meng SW, Mitchell T, Dean RA. 2008. Transcriptome analysis reveals new insight into appressorium formation and function in the rice blast fungus *Magnaporthe oryzae*. *Genome Biology* **9**: R85.

Otsu N. 1979. Threshold selection method from gray-level histograms. *IEEE Transactions on Systems Man and Cybernetics* **9**: 62–66.

Parker D, Beckmann M, Zubair H, Enot DP, Caracuel-Rios Z, Overy DP, Snowdon S, Talbot NJ, Draper J. 2009. Metabolomic analysis reveals a common pattern of metabolic re-programming during invasion of three host plant species by *Magnaporthe grisea*. *Plant Journal* **59**: 723–737.

Parton RM, Fischer S, Malho R, Papasouliotis O, Jelitto TC, Leonard T, Read ND. 1997. Pronounced cytoplasmic pH gradients are not required for tip growth in plant and fungal cells. *Journal of Cell Science* **110**: 1187–1198.

Patkar RN, Ramos-Pamplona M, Gupta AP, Fan Y, Naqvi NI. 2012a. Mitochondrial beta-oxidation regulates organellar integrity and is necessary for

conidial germination and invasive growth in *Magnaporthe oryzae*. *Molecular Microbiology* **86**: 1345–1363.

Patkar RN, Xue YK, Shui GH, Wenk MR, Naqvi NI. 2012b. Abc3-mediated efflux of an endogenous digoxin-like steroidal glycoside by *Magnaporthe oryzae* is necessary for host invasion during blast disease. *PLoS Pathogens* **8**: e1002888.

Patsoukis N, Georgiou CD. 2004. Determination of the thiol redox state of organisms: new oxidative stress indicators. *Analytical and Bioanalytical Chemistry* **378**: 1783–1792.

Qi ZQ, Wang Q, Dou XY, Wang W, Zhao Q, Lv RL, Zhang HF, Zheng XB, Wang P, Zhang ZG. 2012. MoSwi6, an APSES family transcription factor, interacts with MoMps1 and is required for hyphal and conidial morphogenesis, appressorial function and pathogenicity of *Magnaporthe oryzae*. *Molecular Plant Pathology* **13**: 677–689.

Rhee SG, Chang TS, Jeong W, Kang D. 2010. Methods for detection and measurement of hydrogen peroxide inside and outside of cells. *Molecules and Cells* **29**: 539–549.

Ryder LS, Dagdas YF, Mentlak TA, Kershaw MJ, Thornton CR, Schuster M, Chen J, Wang Z, Talbot NJ. 2013. NADPH oxidases regulate septin-mediated cytoskeletal remodeling during plant infection by the rice blast fungus. *Proceedings of the National Academy of Sciences, USA* **110**: 3179–3184.

Samalova M, Johnson J, Illes M, Kelly S, Fricker M, Gurr S. 2013. Nitric oxide generated by the rice blast fungus *Magnaporthe oryzae* drives plant infection. *New Phytologist* **197**: 207–222.

Scherz-Shouval R, Elazar Z. 2011. Regulation of autophagy by ROS: physiology and pathology. *Trends in Biochemical Sciences* **36**: 30–38.

Schwarzlander M, Finkemeier I. 2013. Mitochondrial energy and redox signaling in plants. *Antioxidants & Redox Signaling* **18**: 2122–2144.

Schwarzlander M, Fricker MD, Muller C, Marty L, Brach T, Novak J, Sweetlove LJ, Hell R, Meyer AJ. 2008. Confocal imaging of glutathione redox potential in living plant cells. *Journal of Microscopy* **231**: 299–316.

Scott B, Eaton CJ. 2008. Role of reactive oxygen species in fungal cellular differentiations. *Current Opinion in Microbiology* **11**: 488–493.

Shetty NP, Jorgensen HJL, Jensen JD, Collinge DB, Shetty HS. 2008. Roles of reactive oxygen species in interactions between plants and pathogens. *European Journal of Plant Pathology* **121**: 267–280.

Skamnioti P, Henderson C, Zhang ZG, Robinson Z, Gurr SJ. 2007. A novel role for catalase B in the maintenance of fungal cell-wall integrity during host invasion in the rice blast fungus *Magnaporthe grisea*. *Molecular Plant–Microbe Interactions* **20**: 568–580.

Soundararajan S, Jedd G, Li X, Ramos-Pamplona M, Chua NH, Naqvi NI. 2004. Woronin body function in *Magnaporthe grisea* is essential for efficient pathogenesis and for survival during nitrogen starvation stress. *Plant Cell* **16**: 1564–1574.

Sun CB, Suresh A, Deng YZ, Naqvi NI. 2006. A multidrug resistance transporter in *Magnaporthe* is required for host penetration and for survival during oxidative stress. *Plant Cell* **18**: 3686–3705.

Takemoto D, Tanaka A, Scott B. 2007. NADPH oxidases in fungi: diverse roles of reactive oxygen species in fungal cellular differentiation. *Fungal Genetics and Biology* **44**: 1065–1076.

Talbot NJ, Ebbole DJ, Hamer JE. 1993. Identification and characterization of MGP1, a gene involved in pathogenicity from the rice blast fungus *Magnaporthe grisea*. *Plant Cell* **5**: 1575–1590.

Talbot NJ, Kershaw MJ. 2009. The emerging role of autophagy in plant pathogen attack and host defence. *Current Opinion in Plant Biology* **12**: 444–450.

Tanabe S, Ishii-Minami N, Saitoh K, Otake Y, Kaku H, Shibuya N, Nishizawa Y, Minami E. 2011. The role of catalase-peroxidase secreted by *Magnaporthe oryzae* during early infection of rice cells. *Molecular Plant–Microbe Interactions* **24**: 163–171.

Tanabe S, Nishizawa Y, Minami E. 2009. Effects of catalase on the accumulation of H_2O_2 in rice cells inoculated with rice blast fungus, *Magnaporthe oryzae*. *Physiologia Plantarum* **137**: 148–154.

Temme N, Tudzynski P. 2009. Does *Botrytis cinerea* ignore H_2O_2-induced oxidative stress during infection? Characterization of Botrytis Activator Protein 1. *Molecular Plant–Microbe Interactions* **22**: 987–998.

Thines E, Weber RWS, Talbot NJ. 2000. MAP kinase and protein kinase A-dependent mobilization of triacylglycerol and glycogen during appressorium turgor generation by *Magnaporthe grisea*. *Plant Cell* **12**: 1703–1718.

Thomma BPHJ, Nürnberger T, Joosten MHAJ. 2011. Of PAMPs and effectors: the blurred PTI–ETI dichotomy. *Plant Cell* **23**: 4–15.

Toledano MB, Delaunay-Moisan A, Outten CE, Igbaria A. 2013. Functions and cellular compartmentation of the thioredoxin and glutathione pathways in yeast. *Antioxidants & Redox Signaling* **18**: 1699–1711.

Torres MA. 2010. ROS in biotic interactions. *Physiologia Plantarum* **138**: 414–429.

Tudzynski P, Heller J, Siegmund U. 2012. Reactive oxygen species generation in fungal development and pathogenesis. *Current Opinion in Microbiology* **15**: 653–659.

Urban M, Bhargava T, Hamer JE. 1999. An ATP-driven efflux pump is a novel pathogenicity factor in rice blast disease. *European Molecular Biology Organization Journal* **18**: 512–521.

Valent B, Khang CH. 2010. Recent advances in rice blast effector research. *Current Opinion in Plant Biology* **13**: 434–441.

Veneault-Fourrey C, Barooah M, Egan M, Wakley G, Talbot NJ. 2006. Autophagic fungal cell death is necessary for infection by the rice blast fungus. *Science* **312**: 580–583.

Wang ZY, Soanes DM, Kershaw MJ, Talbot NJ. 2007. Functional analysis of lipid metabolism in *Magnaporthe grisea* reveals a requirement for peroxisomal fatty acid beta-oxidation during appressorium-mediated plant infection. *Molecular Plant–Microbe Interactions* **20**: 475–491.

White NS, Errington RJ, Fricker MD, Wood JL. 1996. Aberration control in quantitative imaging of botanical specimens by multidimensional fluorescence microscopy. *Journal of Microscopy* **181**: 99–116.

Wilson RA, Talbot NJ. 2009. Under pressure: investigating the biology of plant infection by *Magnaporthe oryzae*. *Nature Reviews Microbiology* **7**: 185–195.

Winterbourn CC. 2008. Reconciling the chemistry and biology of reactive oxygen species. *Nature Chemical Biology* **4**: 278–286.

Winterbourn CC, Hampton MB. 2008. Thiol chemistry and specificity in redox signaling. *Free Radical Biology and Medicine* **45**: 549–561.

Xu Q, Liu SY, Zou QJ, Guo XL, Dong XY, Li PW, Song DY, Chen H, Zhao YD. 2009. Microsensor *in vivo* monitoring of oxidative burst in oilseed rape (*Brassica napus* L.) leaves infected by *Sclerotinia sclerotiorum*. *Analytica Chimica Acta* **632**: 21–25.

Yang SL, Lin C-H, Chung K-R. 2009. Coordinate control of oxidative stress tolerance, vegetative growth, and fungal pathogenicity via the AP1 pathway in the rough lemon pathotype of *Alternaria alternata*. *Physiological and Molecular Plant Pathology* **74**: 100–110.

Yoshioka H, Asai S, Yoshioka M, Kobayashi M. 2009. Molecular mechanisms of generation for nitric oxide and reactive oxygen species, and role of the radical burst in plant immunity. *Molecules and Cells* **28**: 321–329.

Supporting Information

Additional supporting information may be found in the online version of this article.

Fig. S1 Functional isolation of septal compartments in developing spores in *Magnaporthe oryzae* measured using fluorescent recovery after photobleaching (FRAP) of Grx1-roGFP2.

Fig. S2 Occlusion of septal pores in developing spores in *Magnaporthe oryzae* observed using transmission electron microscopy.

Methods S1 Transmission electron microscopy of conidia from *Magnaporthe oryzae*.

Video S1 Measurement of the redox potential of the glutathione pool in *Magnaporthe oryzae* germlings using recombinant Grx1-roGFP2.

Video S2 Measurement of reactive oxygen species (ROS) using 2′,7′-dichlorodihydrofluorescein diacetate (H_2DCFDA) in developing spores and during appressorium formation in *Magnaporthe oryzae*.

Video S3 Simultaneous measurement of mitochondrial membrane potential, reactive oxygen species (ROS) and Grx1-roGFP2 ratio in a swelling germ tube of *Magnaporthe oryzae*.

Video S4 Simultaneous measurement of mitochondrial membrane potential, reactive oxygen species (ROS) and Grx1-roGFP2 ratio in a developing appressorium of *Magnaporthe oryzae*.

Video S5 Formation of glutathione-bimane and subsequent vacuolar sequestration in a developing germling of *Magnaporthe oryzae*.

Video S6 Animated three-dimensional projections of vacuolar segmentation in spores of *Magnaporthe oryzae* during the early stages of germination.

Video S7 Animated three-dimensional projections of Grx1-roGFP2 fluorescence expressed in *Magnaporthe oryzae*, and the corresponding ratio images, 16 or 24 h after inoculation on a susceptible rice variety, CO39.

Video S8 Animated three-dimensional projections of Grx1-roGFP2 fluorescence expressed in *Magnaporthe oryzae*, and the corresponding ratio images, 48 h after inoculation on a susceptible rice variety, CO39.

Video S9 Animated three-dimensional projections of Grx1-roGFP2 fluorescence expressed in *Magnaporthe oryzae*, and the corresponding ratio images, 16 or 24 h after inoculation on a resistant rice variety, IR68.

Video S10 Animated three-dimensional projections of Grx1-roGFP2 fluorescence expressed in *Magnaporthe oryzae*, and the corresponding ratio images, 48 h after inoculation on a resistant rice variety, IR68.

Please note: Wiley Blackwell are not responsible for the content or functionality of any supporting information supplied by the authors. Any queries (other than missing material) should be directed to the *New Phytologist* Central Office.